Modeling of Young's modulus variations with temperature of Ni and oxidized Ni using a magneto-mechanical approach

Olivier Hubert, Xavier Milhet, Pascal Gadaud, Mathieu Tatat, Pierre-Olivier Renault, Christophe Coupeau

Modeling of Young's modulus variations with temperature of Ni and oxidized Ni using a magneto-mechanical approach.

Olivier HUBERT[a,*], Xavier MILHET[b], Pascal GADAUD[b], Mathieu TATAT[b], Pierre-Olivier RENAULT[b], Christophe COUPEAU[b]

[a] *LMT-Cachan (ENS-Cachan / CNRS UMR 8535 / Université Paris Saclay), 61 avenue du président Wilson, 94235 CACHAN Cedex, France*
[b] *Institut P´, CNRS-ENSMA-Université de Poitiers, UPR 3346, B.P. 40109, FUTUROSCOPE CHASSENEUIL, Cedex 86961, Poitiers, France*

Abstract

Thin films and coatings are usually used to give functional properties to the surface of the underlying substrate but are never seen as load bearing due to a very low film to substrate thickness ratio. However, this ratio can increase in some specific domains (such as transportation), where the weight reduction is a high stake. This study deals with the influence of the thermally grown oxide (TGO) NiO on the evolution of the elastic modulus of nickel with temperature. For pure nickel, the Young's modulus evolves non-linearly with temperature, from room temperature up to 360°C, corresponding to the Curie temperature of nickel. The amplitude of these variations can be drastically reduced with the presence of the NiO TGO. The purpose of this study is to propose a modeling of these phenomenon using magneto-mechanical approach. A first analytical modeling takes the change of the saturation magnetization, of the initial anhysteretic susceptibility and of the maximal magnetostriction with a relaxation of magneto-crystalline anisotropy concomitant to increasing temperature, into account. The second modeling is a numerical modeling giving the average behavior of a representative volume element. It allows a continuous description of the change with temperature of the Young's modulus and a clear interpretation of the effect of a coating. This gives an insight for future promising applications.

*Corresponding author - hubert@lmt.ens-cachan.fr - ++33 1 47 40 22 24

Keywords: Nickel, Thermally-Grown-Oxide, *Delta* E effect, Magneto-mechanical coupling, Magnetostriction, Multiscale modeling, Residual stresses

1. Introduction

Thin films and coatings are generally used to give functional properties to the surface of the underlying substrate. For example, they play an important role of diffusion barriers to prevent the degradation of the substrate by oxidation when used at high temperature [1]; they can be used to prevent wear and erosion, or to provide lubrication and thermal insulation [2]. Various chemical and/or physical deposition techniques (with various compositions) can be used or they can develop naturally, resulting for example from the oxidation of the surface in a controlled atmosphere (thermally grown oxide TGO) [3]. Generally, these films are very thin and are not seen as load bearing. In some particular applications, such as turbine blades for example, the coating to substrate thickness ratio increases, inducing some peculiar mechanical behaviors as observed for Young's modulus variation of oxidized nickel in a recent study [4, 5]. The elastic modulus has been measured from 20°C up to 600°C. Its evolution with temperature is non-linear and non monotonous from room temperature up to 360°C, corresponding to the Curie temperature of nickel. But the amplitude of these variations can be drastically reduced by the TGO.

The non-monotonous Young's modulus evolution with temperature was previously reported by many authors [6, 7, 8], known as temperature dependent ΔE effect. Its relation with the mechanical or magnetic state of material was discussed in the early work of Bozorth [6] who reported experiments from Siegel, Quimby and Köster [9].

The influence of TGO on this behavior was not reported since the work of Tatat [5] (expect experiments of Huntz interpreted as internal stress rearrangement [10]) and no model was proposed to simulate the variation of pure nickel Young's modulus with temperature and model the influence of the oxide layer on this behavior. Actually, it was suspected to arise from a long-range modification of the internal stresses within the substrate. This interpretation seems accurate considering that stress is well known to change significantly the magnetic behavior [6, 7, 11] and the apparent Young's modulus of a wide range of magnetic materials [12].

The purpose of this paper is to propose a modeling of the variation of Young's modulus of Ni and Ni-NiO layers with temperature using a magneto-mechanical approach. As these approaches usually consider the influence of multiaxial stress on the magneto-mechanical behavior, they allow an accurate modeling of both Young's modulus (seen a stress *vs* strain ratio for a low stress amplitude) and internal stress effect. Experimental results are first reminded. Two modeling approaches are then proposed: an analytical modeling first based on a room temperature ΔE effect modeling [12]; a numerical implementation is secondly detailed based on the work of Daniel [13] allowing a continuous description of the Young's modulus variations with temperature and taking the TGO, or any other coating nature leading to residual stresses, into account.

2. Experimental results and interpretation

2.1. Material and experimental features

A pure (>99%) 2 mm thick polycrystalline nickel has been used for the experimental study [4, 5]; the initial grain size of the Ni samples is about 30 μm. After a soft mechanical polishing, samples have been oxidized in synthetic air (80% nitrogen, 20% oxygen) during 1h30 at 1110°C to form NiO coatings and then furnace cooled at approximately 300°C/h. The specimen was exposed to an $Ar - H_2$ flow to limit the oxidation prior to the target temperature and during cooling. The oxidation was simultaneously performed on the two opposite free surfaces of the Ni samples. After oxidation, the thickness of the NiO coatings has been estimated at 16 μm thick (figure 1). Electron Back Scattered Diffraction (EBSD) measurements were carried out on a polished sample after oxidation (for a 40mm^2 area - 10mm $\times$ 4mm). Figure 2 shows a typical example of inverse pole figure (with respect to the normal direction ND) obtained after oxidizing. The grain size of the Ni substrate has evolved substantially by growing up to about 280 μm. Texture index concludes on the other hand to a quasi-isotropic distribution of orientations: the material can be considered as isotropic.

The elastic properties of the specimens were investigated from room temperature (RT) up to 600°C by means of the resonant frequency technique in bending mode [14] in the 1-10 kHz range (the temperature range 20°C to 600°C was chosen in order to make sure to measure the material behavior

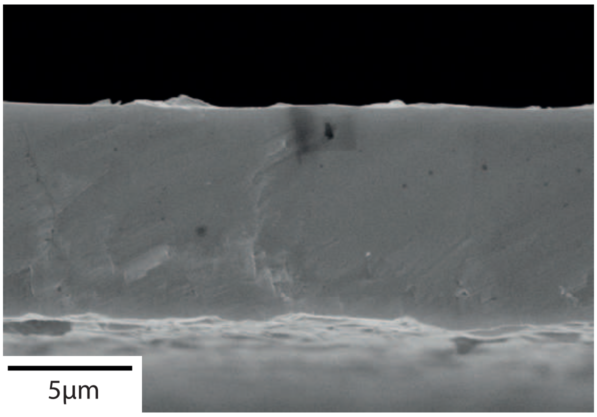

Figure 1: SEM observation of typical NiO oxide layer after oxidizing in synthetic air during 1h30 at 1110°C.

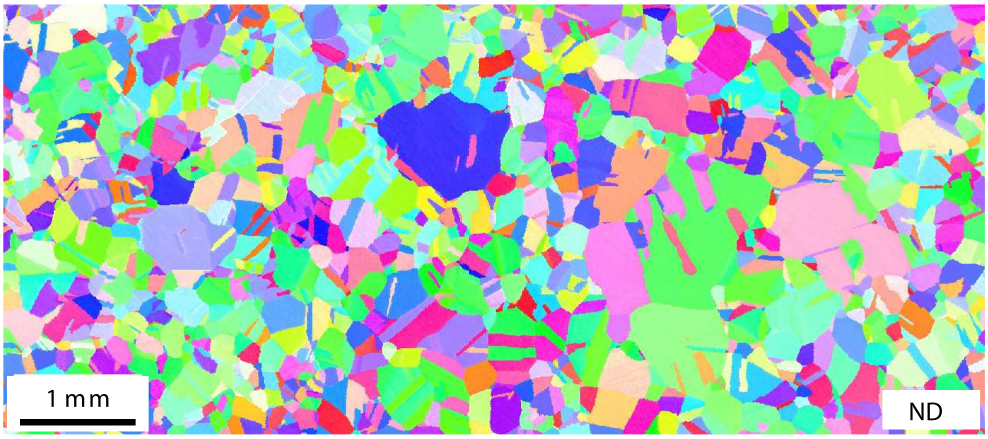

Figure 2: Inverse pole figure (normal direction ND) obtained by EBSD on the Ni sample after oxidizing treatment.

well above the Curie temperature). This method is detailed hereafter: In the case of a bulk material, the longitudinal Young's modulus (E) can be deduced using the following relation [15]:

$$E = 0.9464\rho f^2 \frac{L^4}{h^2}\zeta \tag{1}$$

where f is the flexural resonance frequency, ρ the density, h and L, the beam thickness (0.5 to 2 mm) and span length (20 to 30 mm), and ζ, a correcting factor close to 1. The sample is maintained horizontally between steel wires located at the vibration nodes. Both excitation and detection are performed using an electrostatic device (capacitance created between the sample and a unique electrode). Using this set-up, the Young's modulus can be measured from -150°C up to 1100°C without any harmful contact. The heating rate can be as low as 1°C/min and high vacuum ($\approx 10^{-4}$ Pa) is used to hinder or limit the specimen oxidation. The accuracy of this method is better than 0.5% for conductive bulk materials whatever the rigidity range. An important feature of this technique lies in the very low applied stress level, less than 1 MPa.

2.2. Variation of Young's modulus

Figure 3 shows the evolution of the Young's modulus of the specimens with temperature [4]. The measurements reported here were performed using the same Ni substrate; the Young's modulus was first measured on the laminated state before oxidation, secondly on the two-sides oxidized specimen (*i.e.* two NiO coatings) and, finally, after removing one and both NiO coatings successively by fine polishing (noted as "peeled off samples" in the following). The procedure to remove the oxide, based on conventional metallographic techniques, included an ultimate step of fine chemo-mechanical polishing in order to reach a very low roughness without work hardening *i.e.* no additional residual stresses in the sub-surface.

Two domains are clearly evidenced in figure 3, depending on the temperature. Above approximately T = 360°C, the evolution of the elastic modulus is quite similar regardless to the specimen state, characterized by the expected linear decrease of the Young's modulus with the temperature. A slight difference between non-oxidized and oxidized substrates can be observed due to composite effect: the Young's modulus of NiO is usually higher than the Young's modulus of pure Ni; its value depends strongly on oxidizing temperature and oxide porosity [4]. It must be emphasized that the increase of the grain size from 30 to 280 μm does not act on the modulus of the substrate (the experimental technique integrates all the sample volume).

Below this threshold temperature, the Young's modulus depends strikingly on the structural configuration of the specimens:

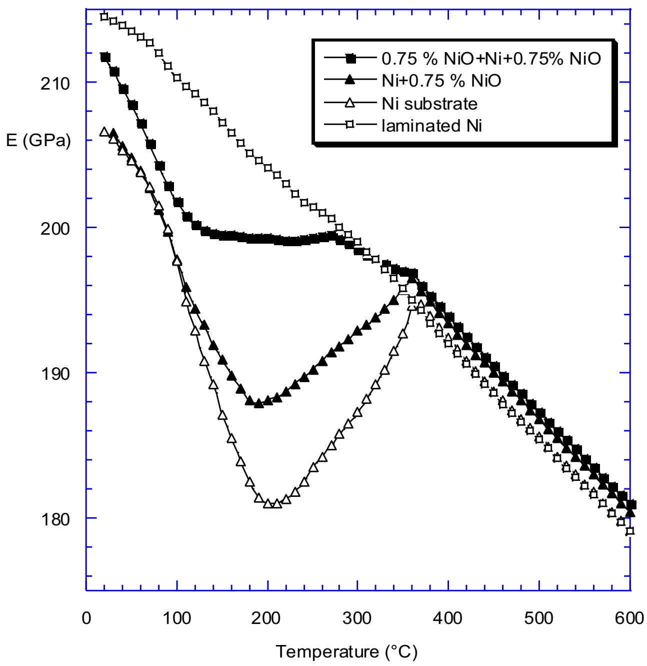

Figure 3: Variation of Young's modulus with temperature for different specimens.

- the presence of the NiO oxide layer representing only about 3% of the total thickness on the Ni substrate significantly influences the value of the elastic modulus (apparent Young's modulus E_a) at a temperature range between 90°C and 360°C.

- the variation of the Young's modulus at 260°C for oxidized samples can be associated to the Néel temperature transition of NiO.

- the maximum deviation of E_a is about 9% between nickel and nickel-oxide.

2.3. Estimation of residual stresses

The residual stresses have been determined at RT using the X-ray diffraction (XRD) so-called $sin^2\psi$ method [16] where ψ is defined as the angle between the normal to the sample surface and the normal to the diffracting planes. X-ray measurements were carried out using a four-circle diffractometer (Seifert XRD 3003) operating at 40 kV and 40 mA, with a Cu X-ray tube ($\lambda_{K\alpha}$= 0.15418 nm) equipped with a 1×1 mm^2 point focus and a Ni filter on the direct beam path to absorb the Cu $K\alpha$ radiation. The incident beam was collimated using a collimator 1 mm in diameter and targeted on the samples mounted on an Eulerian cradle for ψ tilting. The X-ray measurements have been performed for fourteen different ψ angles for two independent plane families, namely {331} and {420}. The residual stress state was calculated from the lattice strains assuming a planar equibiaxial stress state and using the X-ray elastic constants [17]. For a polycrystalline quasi-isotropic material of Young's modulus E and Poisson's ratio ν, the biaxial residual stress state of magnitude σ^r is given by the slope of $sin(\theta)^{-1} = f(sin^2\psi)$ function following:

$$\frac{sin(\theta_0)}{sin(\theta)} = \sigma^r(\frac{(1+\nu)sin^2\psi - 2\nu}{E}) + 1 \tag{2}$$

where θ and θ_0 indicate the Bragg's angle of the diffracting plane with or without stress respectively. The technique was used to evaluate the residual stress level inside both the as-received material and the material after oxidation [5]. In the as-received state the material exhibits a high level of residual stress in sub-surface that corresponds to a biaxial compression of amplitude -130±30 MPa. This surface stress state should be equilibrated by an internal bi-tension stress that can unfortunately not be estimated because the transition area between these two fields cannot clearly be defined. It can be considered that thermal treatment completely reduces this stress field to zero since a global recrystallization mechanism occurs.

After oxidation, the internal stresses have only been determined in the NiO coatings. Actually the X-Ray diffraction analysis is not possible in the Ni layer due to the large grain size. Internal stresses in NiO correspond to an equibicompression of amplitude -550±50 MPa [5]. Similar compressive stresses values are reported in literature [10, 19]. They mainly result from the thermal mismatch coefficients between the coating and the substrate. Indeed dilatation coefficients for NiO and Ni are respectively: α_{NiO} =14.5×10^{-6}K^{-1} and α_{Ni} =17.5×10^{-6}K^{-1} [18, 19]. The thermal stresses distribution in the Ni layer has been determined from a simple beam analysis integrating the experimental values obtained for the oxide coatings thickness and residual stress, and considering a global equilibrium (force and momentum equilibrium). For NiO-Ni-NiO system, the in-plane stress in the Ni substrate is a bi-tension and remains constant over the entire thickness (+9±1 MPa), while for Ni-NiO the stress decreases linearly from a bi-tension (+18±2 MPa) to a bi-compression state (-9±1 MPa) giving an average value of +3±1 MPa. After removal of the double oxide coating, it may be assumed that the Ni layer is completely internal stress free.

As seen in figure 3 and table 1, internal stresses of few MPa are sufficient to significantly modify the apparent Young's modulus of nickel. Results reported in table 1 correspond to the estimated average biaxial stress inside the Ni Layer.

Table 1: Change of ΔE effect with biaxial residual stress level of amplitude σ^r.

Configuration	Cold rolled	2-sides oxidized	1-side oxidized	Peeled-off
ΔE/E(%)	0	-3	-8	-11
σ^r(MPa)	unknown	+9	+3 (average)	0

2.4. Results interpretation

The non monotonous change of Young's modulus with temperature and effect of TGO cannot be explained by a classical mechanical rule of mixture but by magneto-elastic considerations. Ni is a ferromagnetic material exhibiting magnetic domains below its Curie temperature, T_C, equal to 360°C [6].

The observed evolution of pure Ni Young's modulus for increasing temperature was already experimentally reported in literature [6, 7, 8]. This deviation from the Hooke's law is known as the ΔE effect ("Δ" for variation) and can only be highlighted in the very first stage of stress-strain curves [13]. A relation with the magnetic character of the material can be made considering:

1. The phenomenon is strongly dependent on the magnetization M of the layer: at the magnetic saturation ($M = M_s$; M_s: saturation magnetization of the material) the non-linear variation of Young's modulus progressively vanishes.

2. Young's modulus recovers its linear variation with temperature above the Curie temperature of the layer (360°C).

These points are illustrated in figure 4a.

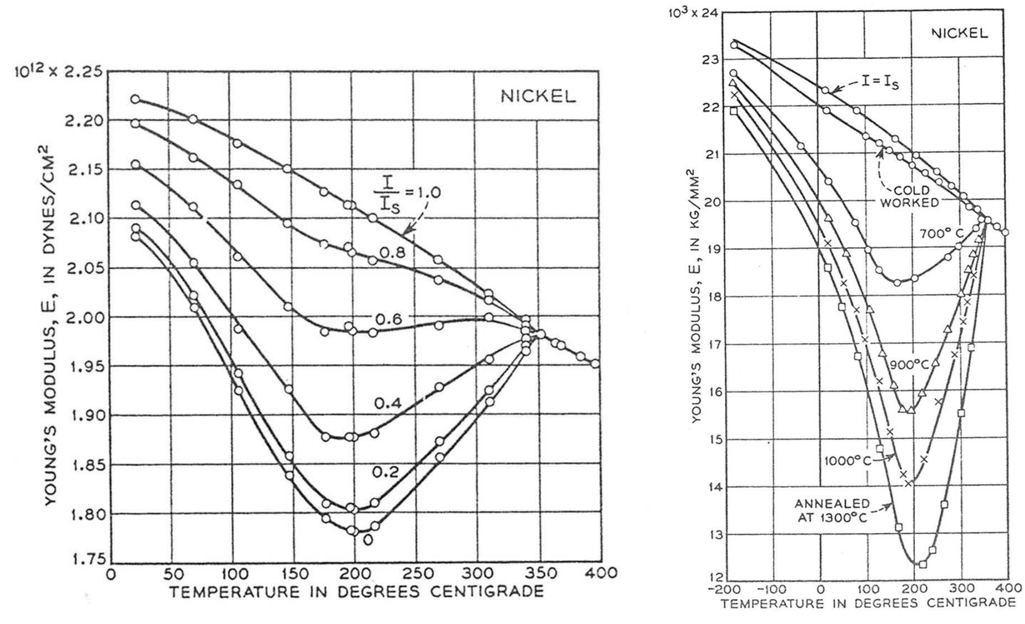

(a) (b)

Figure 4: Apparent Young's modulus of nickel vs. Temperature: (a) effect of magnetization to saturation magnetization ratio (I/I_s); (b) effect of mechanical condition ("internal stress") and thermal annealing [6] - NB: 10^{12}[Dynes/cm^2]=10^2[GPa]; 10^3[Kg/mm^2]=9.81[GPa]$\approx$ 10[GPa].

As magnetic properties of ferromagnetic materials depend on the temperature, the amplitude of ΔE effect can change. In particular, the magnetocrystalline anisotropy (determining for a single crystal the most favorable magnetization direction) decreases significantly while the temperature increases, especially from RT up to 100°C for Ni [6]. Hence, with increasing temperature, the magnetic moments direction becomes progressively more sensitive to the mechanical stress, enhancing the ΔE effect. From approximately T= 200°C to the Curie temperature, the spontaneous magnetization (and consequently the magnetostriction) of Ni quickly decreases down to 0: the ferromagnetic properties disappear (magnetostrictive and exchange constants progressively decrease to zero). This latter point explains that the ΔE effect is gradually weakened and vanishes at T_C when the material becomes paramagnetic.

The role of stress is another point to consider. For cold worked nickel (as received material), the decrease of Young's modulus is regular following a classical linear variation with temperature (figure 3). Thermal annealing at increasing temperature progressively enhances the non-linear phenomenon as experimentally observed and reported in figure 4b [6]. The internal stress associated to plasticity acts as a magnetic saturation; the stress relieving at increasing annealing temperature acts as a demagnetization. The effect of oxide layers is another typical example of coupling to stress. X-rays measurements indicates that the substrate is submitted to residual stresses. Single-layer or two-layers situations do not lead to the same stress level. The amplitude of non-linearity of Young's modulus is changed. The highest amplitude of ΔE effect is reached for peeled off sample where residual stress reduces to zero.

Considering finally that the measurement method is based on a stress loading, a quantitative modeling of these phenomena requires to use a fully coupled magneto-mechanical approach and to consider the effect of temperature on the parameters involved in this coupling.

3. Modeling

3.1. ΔE effect definition

The so-called ΔE effect is one of the manifestations of magneto-elastic couplings in ferromagnetic materials [7]. It can be defined as the dependence of Young's modulus E of a material on its state of magnetization. The Young's modulus of an originally demagnetized specimen appears to be lower (by an amount ΔE) than the Young's modulus of the same specimen magnetized at saturation (figure 5). Indeed a ferromagnetic material is subdivided in magnetic domains. A magnetic domain corresponds to microscopic organization of magnetic moments aligned together to minimize the so-called exchange energy. Each magnetic domain is magnetized at saturation and characterized by a free isochoric strain called magnetostriction. Due to magneto crystalline energy, orientation of magnetic domains is usually associated to crystallographic axes (8 easy directions for nickel - 8 domain families). At zero applied stress or magnetic field and without boundary effect, domains are equally distributed so that the initial deformation and magnetization are null. An increasing magnetic field leads to a progressive increase of the well oriented domain families volume so that macroscopic magnetization and deformation occur (macroscopic magnetostriction ϵ^μ). An increasing uniaxial stress σ leads to a progressive increase of the well oriented domain families of opposite sign so that a macroscopic magnetostriction ϵ^μ occurs while macroscopic magnetization remains null.

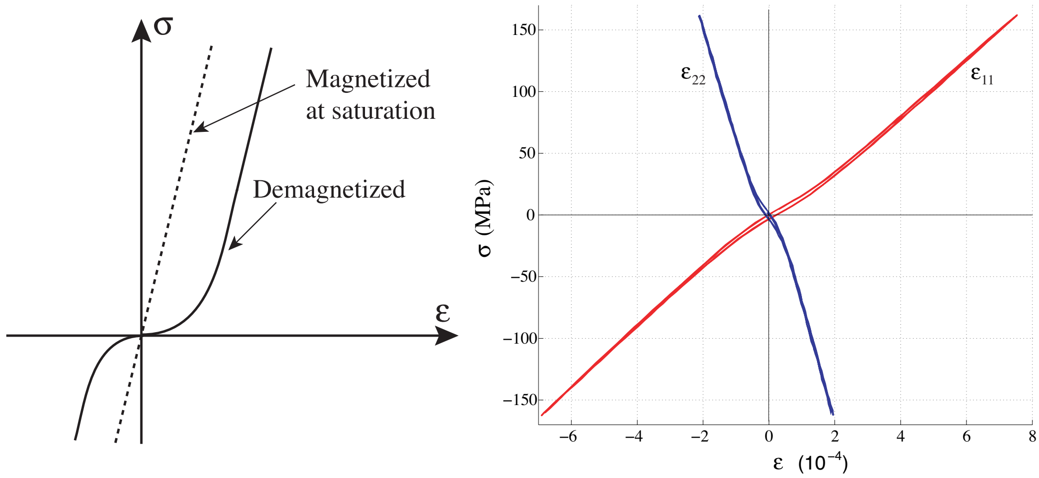

Figure 5: Illustration of the ΔE effect for a tensile-compressive test (ϵ is the total strain); (a) principle (b) illustration for iron-cobalt alloy [20].

This magnetostriction strain ϵ^μ is superimposed to the elastic strain ϵ^{el}, so that the total measured strain ϵ is higher than foreseen without magnetostriction phenomenon. It is defined by equation (3), all the strains being measured in the direction parallel to the applied stress.

$$\epsilon = \epsilon^\mu + \epsilon^{el} \tag{3}$$

Because ϵ^μ is usually non-linear with stress and saturates, the apparent Young's modulus appears non-linear and saturates too. The stress level investigated using the resonant technique for measurement of Young's modulus is very small (<1MPa). The apparent Young's modulus E_a is given by:

$$E_a = \left(\left. \frac{d\epsilon^\mu}{d\sigma} \right|_{\sigma=0} + \left. \frac{d\epsilon^{el}}{d\sigma} \right|_{\sigma=0} \right)^{-1} \tag{4}$$

In case of a saturated material, the magnetic domain structure has reached a saturated configuration and the magnetostriction strain cannot evolve anymore. The apparent Young's modulus is then defined as:

$$E_a = \left.\frac{d\sigma}{d\epsilon^{el}}\right|_{\sigma=0} \tag{5}$$

leading to a higher value because $\frac{d\epsilon^{\mu}}{d\sigma}$ is always positive [12]. This phenomenon is described by Bozorth [6] and reported in figure 4. In case of a highly deformed material, the internal stresses saturate the magnetostriction leading to the same effect.

3.2. Analytical modeling of apparent Young's modulus

An analytical modeling of the ΔE effect at RT has been recently proposed [12]. This approach is inspired from a multiscale model for the prediction of magneto-elastic reversible behavior of ferromagnetic materials presented in [13] and in Appendix A. The full multiscale model is used for a numerical resolution in section 4. The simplified approach is limited to the situation where no magnetic field is applied, so that the magneto-static energy does not appear in the definition of the magnetic equilibrium. On the other hand it has been supposed that the magneto-crystalline anisotropy energy does not participate to the evolution of the magnetostriction strain. In such conditions, the elastic energy is the only energy term explicitly considered in the description of the magnetic equilibrium of a domain.

On the other hand, an isotropic polycrystal can be seen as an aggregate of single crystals with random orientation. Polycrystal can be considered as a single crystal for which all directions would be easy directions. In one domain of such a single crystal, the magnetostriction strain tensor can be written (in its own framework):

$$\boldsymbol{\epsilon}^{\mu}_{m} = \frac{1}{2}\lambda_{max}\begin{pmatrix} 2 & 0 & 0 \\ 0 & -1 & 0 \\ 0 & 0 & -1 \end{pmatrix} \tag{6}$$

λ_{max} denotes the maximum magnetostriction strain of the considered polycrystal.

A multiaxial eigen-stress tensor is considered in the macroscopic frame $(\vec{e}_1, \vec{e}_2, \vec{e}_3)$ following:

$$\boldsymbol{\sigma} = \begin{pmatrix} \sigma_{11} & 0 & 0 \\ 0 & \sigma_{22} & 0 \\ 0 & 0 & \sigma_{33} \end{pmatrix} \tag{7}$$

The transformation matrix from macroscale to domain scale is given by:

$$\boldsymbol{P} = \begin{pmatrix} \cos\theta \sin\varphi & \sin\theta & \cos\theta \cos\varphi \\ \sin\theta \sin\varphi & -\cos\theta & \sin\theta \sin\varphi \\ \cos\varphi & 0 & -\sin\varphi \end{pmatrix} \tag{8}$$

leading to:

$$\boldsymbol{\epsilon}_p^\mu =^t \boldsymbol{P}\, \boldsymbol{\epsilon}_m^\mu\, \boldsymbol{P} \tag{9}$$

The magneto-elastic energy is given for a constant by:

$$W_\sigma^\alpha = -\boldsymbol{\sigma} : \boldsymbol{\epsilon}_p^\mu \tag{10}$$

that can be expressed as function of strain and stress components following:

$$W_\sigma^\alpha = -\frac{\lambda_{max}}{2}\big(\sigma_{11}(3\cos^2\theta \sin^2\varphi - 1) + \sigma_{22}(3\sin^2\theta \sin^2\varphi - 1) + \sigma_{33}(3\cos^2\varphi - 1)\big) \tag{11}$$

Angles θ (0-2π) and φ (0-π) define the orientation of domain in the macroscopic frame.

Considering homogeneous stiffness, localization operation is avoided. The average magnetostriction is given by:

$$\boldsymbol{\epsilon}^\mu = \int_\alpha f_\alpha \boldsymbol{\epsilon}_p^\mu \tag{12}$$

f_α indicates the volume fraction of domain α (see equation A.8 in Appendix A) calculated using:

$$f_\alpha = \frac{\exp(-A_s.W_\sigma^\alpha)}{\displaystyle\int_0^{2\pi}\int_0^{\pi} \exp(-A_s.W_\sigma^\alpha)\ \sin\varphi\, d\varphi\, d\theta} \tag{13}$$

with (see equation A.11 in Appendix A):

$$A_s = \frac{3\chi_0(T)}{\mu_0 M_s(T)^2}\frac{T^{RT}}{T} \tag{14}$$

χ_0 and M_s are the initial anhysteretic susceptibility (variation of anhysteretic magnetization with magnetic field) and saturation magnetization. μ_0 is the vacuum permeability (=$4\pi \times 10^{-7}$ Henry/m). T indicates the actual temperature and T^{RT} the room temperature.

A tensile test of magnitude σ along the macroscopic unit vector $\vec{e}_3$ is now considered. The magneto-elastic energy expression is simplified into:

$$W_\sigma^\alpha = -\frac{1}{2}\lambda_{max}\sigma\left(3\cos^2\varphi - 1\right) \tag{15}$$

The magnetostriction strain tensor is diagonal:

$$\boldsymbol{\epsilon}^\mu = \frac{\pi\,\lambda_{max}\,S_2}{2\,S_1}\exp(-\frac{1}{2}A_s\lambda_{max}\sigma)\begin{pmatrix} -1 & 0 & 0 \\ 0 & -1 & 0 \\ 0 & 0 & 2 \end{pmatrix} \tag{16}$$

with

$$S_1 = 2\pi\exp(-\frac{1}{2}A_s\lambda_{max}\sigma)\int_0^\pi \exp(\frac{3}{2}A_s\lambda_{max}\sigma\cos^2\varphi)\sin\varphi\,d\varphi \tag{17}$$

and,

$$S_2 = \int_0^\pi (3\cos^2\varphi - 1)\exp(\frac{3}{2}A_s\lambda_{max}\sigma\cos^2\varphi)\sin\varphi\,d\varphi \tag{18}$$

The apparent Young's modulus is measured by the resonance method corresponding to a low magnitude tensile loading. Considering the additivity of deformation (homogeneous stress) at a physical point, the apparent Young's modulus verifies:

$$\frac{1}{E_a} = \frac{1}{E} + \frac{1}{E_m} \tag{19}$$

with E the ideal Young's modulus and E_m the magnetostriction modulus. The latter satisfies:

$$\frac{1}{E_m} = \left.\frac{d\epsilon_{33}^\mu}{d\sigma}\right|_{\sigma=0} \tag{20}$$

Since an analytical expression of magnetostriction *vs* stress is available, the calculation is developed:

$$\epsilon_{33}^{\mu} = \frac{\pi\,\lambda_{max}\,S_2(\sigma)}{S_1(\sigma)}\exp(-\frac{1}{2}A_s\lambda_{max}\sigma) \tag{21}$$

A derivation of ϵ_{33}^{μ} function with respect to stress at $\sigma = 0$, leads to, after few calculations:

$$\frac{1}{E_m} = \left.\frac{d\epsilon_{33}^{\mu}}{d\sigma}\right|_{\sigma=0} = \frac{\lambda_{max}^2 A_s}{5} = \frac{3\chi_0(T)\lambda_{max}^2}{5\mu_0 M_s(T)^2}\frac{T^{RT}}{T} \tag{22}$$

Most of the terms are temperature dependent, including λ_{max}, that may lead to a complex variation of the magnetostriction modulus with temperature. It is possible to extend the proposed approach to other hypotheses than homogeneous stiffness by reporting the localization operation in the definition of λ_{max}. This point is addressed in the next section.

3.3. Numerical applications for pure isotropic polycrystalline nickel and influence of temperature

The parameter λ_{max} can be derived from magnetostrictive constants of single crystal λ_{100} and λ_{111} following different assumptions, depending of either or not the magnetization rotation is considered, and depending on the elastic behavior of the domain (single crystal stiffness constants) and the average medium. An analytical calculation of the average magnetostrictive tensor can be strictly made only at magnetic saturation, when the magnetization is uniformly aligned along the external field direction. Grains g are composed of single domains α so that the magnetostriction strain in each grain is the magnetostriction strain of the domain in the crystallographic frame (CF) :

$$\boldsymbol{\epsilon}_{\mu}^{g} = \boldsymbol{\epsilon}_{\mu}^{\alpha} = \frac{3}{2}\begin{pmatrix} \lambda_{100}(\gamma_1^2 - \frac{1}{3}) & \lambda_{111}\gamma_1\gamma_2 & \lambda_{111}\gamma_1\gamma_3 \\ \lambda_{111}\gamma_1\gamma_2 & \lambda_{100}(\gamma_2^2 - \frac{1}{3}) & \lambda_{111}\gamma_2\gamma_3 \\ \lambda_{111}\gamma_1\gamma_3 & \lambda_{111}\gamma_2\gamma_3 & \lambda_{100}(\gamma_3^2 - \frac{1}{3}) \end{pmatrix}_{CF} \tag{23}$$

The average magnetostriction strain is the solution of a thermo-elasticity problem [21]:

$$\boldsymbol{\epsilon}_{\mu}^{sat} = <{}^t\mathbb{B}^g : \boldsymbol{\epsilon}_{\mu}^{g}> \tag{24}$$

where ${}^{t}\mathbb{B}^{g}$ indicates the transpose of the stress concentration tensor and $< .. >$ denotes the averaging operation over the volume. The macroscopic behavior being isotropic, previously defined equation (6) gives the average saturation magnetostriction strain tensor with $\lambda_{max} = \lambda_{sat}$ the saturation magnetostriction. In case of high magneto crystalline anisotropy, domain wall displacement and magnetization rotation can be considered as successive (they are usually considered as concomitant) so that it is possible to estimate another average magnetostriction tensor denoted average *maximal* magnetostriction strain tensor. A calculation of analytical values is possible using $\lambda_{100} = 0$ for $< 111 >$ easy directions materials or $\lambda_{111} = 0$ for $< 100 >$ easy directions materials:

- in case of low magneto crystalline energy (free rotation) or at the magnetic saturation:

$$\lambda_{max} = \lambda_{sat} = \frac{2}{5}\lambda_{100}k^{a} + \frac{3}{5}\lambda_{111}k^{b}$$

  This value corresponds to the theoretical magnetostriction at the magnetic saturation.

- in case of high magneto crystalline energy (no rotation):

$$\begin{aligned} \lambda_{max} &= \tfrac{2}{5}\lambda_{100}k^{a} \quad \text{for materials with} \\ & \qquad\qquad\quad < 100 > \text{easy directions} \\ \lambda_{max} &= \tfrac{3}{5}\lambda_{111}k^{b} \quad \text{for materials with} \\ & \qquad\qquad\quad < 111 > \text{easy directions} \end{aligned}$$

k^{a} and k^{b} are homogenization parameters depending on the elastic properties. They are given by:

$$\left\{ \begin{array}{lcl} k^{a} & = & \dfrac{\mu_a}{\mu_{eff}} \dfrac{\mu_{eff} + \mu^{\star}}{\mu_a + \mu^{\star}} \\ k^{b} & = & \dfrac{\mu_b}{\mu_{eff}} \dfrac{\mu_{eff} + \mu^{\star}}{\mu_b + \mu^{\star}} \end{array} \right. \tag{25}$$

μ_a and μ_b are the the single crystal shear moduli (equation 26 - with C_{ij} the stiffness constants of the cubic symmetry single crystal). μ_{eff} is the shear modulus of the effective medium given by equation (27). $\mu^{\star}$ (eq. 28) is the Hill's shear modulus, whose definition depends on μ_o and κ_o the shear and compression moduli of the reference medium supposed isotropic (NB: $\kappa_o = \kappa$).

$$\left\{ \begin{array}{lcc} \mu_a & = & \frac{1}{2}(C_{11} - C_{12}) \\ \mu_b & = & \frac{1}{2}(C_{44}) \\ \kappa & = & \frac{1}{3}(C_{11} + 2C_{12}) \end{array} \right. \tag{26}$$

$$\mu_{eff} = \frac{5(\mu_a + \mu^\star)(\mu_b + \mu^\star)}{(3\mu_a + 2\mu_b + 5\mu^\star)} - \mu^\star \tag{27}$$

$$\mu^\star = \frac{1}{6}\mu_o \frac{9\kappa_o + 8\mu_o}{\kappa_o + 2\mu_o} \tag{28}$$

The value of these parameters (and finally of k^a and k^b) depends on the homogenization approximations made:

- Homogeneous stress (Reuss hypothesis - *ie*: μ_o=0): $k^a = k^b = 1$
- Homogeneous deformation (Voigt hypothesis - *ie*: $\mu_o = \infty$): $k^a = 5\mu_a/(2\mu_a + 3\mu_b)$ and $k^b = 5\mu_b/(2\mu_a + 3\mu_b)$
- Hashin and Shtrikman upper estimation (*ie*: $\mu_o = \mu_b$ - considering that $\mu_b > \mu_a$)
- Hashin and Shtrikman lower estimation (*ie*: $\mu_o = \mu_a$ - considering that $\mu_b > \mu_a$)
- Self-consistent estimation (*ie*: $\mu_o = \mu_{eff}$ so that μ_{eff} is the result of the self-consistent equation:

$$8\mu_{eff}^3 + (9\kappa + 4\mu_a)\mu_{eff}^2 - (12\mu_a\mu_b + 3\kappa\mu_b)\mu_{eff} - 6\kappa\mu_a\mu_b = 0 \tag{29}$$

Analytical expressions of k_a and k_b are not reported for the three last estimations due to their complicated expressions.

3.3.1. Apparent Young's modulus at the room temperature

The physical constants for nickel used for the calculations are reported in table 2. They are given at RT. The value of the second magneto crystalline constant K_2 strongly varies from one author to another (from one value to its opposite) [6, 7]. The effect of this term is usually negligible when its amplitude is close or inferior to the amplitude of the first magneto crystalline constant K_1. Equation (30) gives the magneto crystalline energy expression function of constants K_1 and K_2 and direction cosines γ_i of magnetization in the crystal frame.

$$W_K^\alpha = K_1(\gamma_1^2\gamma_2^2 + \gamma_2^2\gamma_3^2 + \gamma_3^2\gamma_1^2) + K_2(\gamma_1^2\gamma_2^2\gamma_3^2) \tag{30}$$

The magneto elastic energy can be calculated for a uniaxial stress σ_u along the direction [100] of the single crystal and a magnetostriction strain at the domain scale (23). It gives:

$$W_\sigma^\alpha = -\frac{1}{2}\lambda_{100}\sigma_u\left(3\ \gamma_1^2 - 1\right) \tag{31}$$

To estimate if rotation has to be or not taken into account at RT, a material with positive K_1 ($< 100 >$ easy magnetization direction) and a magnetization rotation of angle θ in the $(\vec{e}_1, \vec{e}_2)$ plane are considered. The magnetoelastic and magnetocrystalline energy of a domain α_1 oriented along $\vec{e}_1$ can be written following:

$$\left\{ \begin{array}{lcl} W_K^{\alpha_1} & = & K_1(cos\theta^2 sin\theta^2) \\ W_\sigma^{\alpha_1} & = & -\frac{1}{2}\lambda_{100}\sigma_u(3cos\theta^2 - 1) \end{array} \right. \tag{32}$$

If no other magnetization mechanism or energy is considered, the variation of total energy is null at equilibrium so that:

$$\frac{dW_K^{\alpha_1}}{d\theta} = -\frac{dW_\sigma^{\alpha_1}}{d\theta} \tag{33}$$

An equalization of the two expressions for $\theta = 0$ allows to estimate an uniaxial stress amplitude σ_u able to initiate a magnetization rotation. Its expression is reported in equation (34).

$$\sigma_u \approx \left| \frac{2K_1}{3\lambda_{100}} \right| \tag{34}$$

Using the numerical values reported in table 2, a stress σ_u higher than 100 MPa is obtained. This value is much larger than the value expected during the Young's modulus measurements (less than 1 MPa). The no rotation assumption can be made at RT so that λ_{max} is defined by:

$$\lambda_{max} = \frac{3}{5}\lambda_{111}k_b \tag{35}$$

Table 2: Physical constants of pure nickel at RT [6, 7]; see figure 10 for χ_0 value.

K_1	K_2	M_s	λ_{100}	λ_{111}	χ_0	C_{11}	C_{12}	C_{44}
-5×10^3	$\pm\ 2\times10^3$	4.84×10^5	-50	-25	800	246	147	248
$J.m^{-3}$	$J.m^{-3}$	A/m	ppm	ppm	-	GPa	GPa	GPa

Assuming finally an effective Young's modulus E of 223 GPa (in accordance with C_{ij} values), different estimations of the apparent Young's modulus can be made depending on the different estimations of k_b. They are reported in the following table:

Table 3: Different estimations of k_b, λ_{max}, E_m, E_a and $\Delta E/E(\%) = (E_a - E)/E \times 100$ at RT - magnetostriction is given in ppm ($\times10^{-6}$) and moduli in GPa - V: Voigt estimation, R: Reuss estimation, HS+: Hashin-Shtrikman upper estimation, HS-: Hashin-Shtrikman lower estimation, SC: self-consistent estimation.

	V	HS+	SC	HS-	R
k_b	1.316	1.209	1.187	1.151	1
λ_{max}	-19.7	-18.1	-17.8	-17.3	-15.0
E_m	1573	1866	1934	2057	2726
E_a	195	199	200	201	206
$\Delta E/E(\%)$	-12.4	-10.7	-10.3	-9.8	-7.6

The sequence of estimations reported in the table is classical. Values are roughly consistent with the experimental results reported in figure 3 and [5, 6]. The homogeneous stress hypothesis giving an apparent Young's modulus of 206 GPa leads nevertheless to the best result. Since the EBSD measurement did not reveal any crystallographic texture, this result could be linked to an anisotropic distribution of domains.

3.3.2. Effect of increasing temperature on apparent Young's modulus

Temperature has a significant effect on the physical constants of nickel used in the analytical modeling.

- Figure 6 shows the experimental results obtained by Kirkham [22] and Döring reported in [6] for the magnetostriction of a polycrystalline nickel (confirmed by the more recent measurements of Tatsumoto [23]). Magnetostriction is decreasing with increasing temperature. It reaches zero at T_C. No data are available for single crystal parameters λ_{100} and λ_{111}. One admissible assumption is to suppose that they behave similarly than the saturation magnetostriction of the isotropic medium. λ_{max} would evolve similarly.

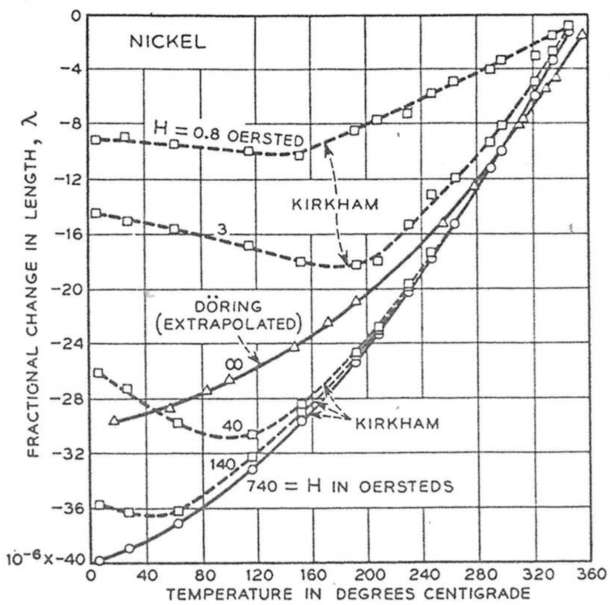

Figure 6: Effect of temperature on the magnetostriction of polycrystalline nickel [6, 22].

- Figure 7 shows the experimental results obtained by Honda [6] and Tatsumoto [24] for the magnetocrystalline constants of nickel. The amplitude of constants decreases drastically with increasing temperature. K_1, initially negative, reaches zero at approximatively 100°C for Honda or 200°C for Tatsumoto, then becomes slightly positive before coming back to zero close to T_C. K_2 is positive and of lower amplitude than K_1. It decreases regularly to zero when temperature is approaching T_C.

- Figure 8 shows the experimental results obtained by Kneller and reported by Ascher [25] for the saturation magnetization of nickel. The decrease of M_s with temperature is much less regular than magnetostrictive and magneto crystalline constants. M_s remains high up to a high temperature level. It drastically decreases to zero when the temperature approaches T_C.

- Finally, figure 9 shows the experimental results obtained by Kirkham [22] for the initial susceptibility of nickel. A global strong increase of susceptibility before a sharp decrease at T_C is observed. The initial increasing is strongly modified by a non monotonous evolution at a temperature (local maximum at T $\approx$ 200°C) that is interpreted by Kirkham as a direct effect of the change of K_1 sign (modifying the easy magnetization axis from the $< 111 >$ to the $< 100 >$ direction). The evolution of this term can be seen as a result of a new magnetic equilibrium associated to new physical constants, as for Young's modulus. It must be noticed that the susceptibility used in the analytical modeling is the *anhysteretic* initial susceptibility, but the data reported are the initial susceptibility of the first magnetization curve. Figure 10 reports the typical cyclic and anhysteretic behaviors of pure polycrystalline nickel measured at RT. The initial susceptibility of the first magnetization curve is drastically different from initial susceptibility of the anhysteretic curve. At RT, initial susceptibility of the first magnetization curve is close to 60 (in accordance with Kirkham measurements) while initial susceptibility of the anhysteretic curve is at minimum ten times higher (about 800). The variations with temperature of initial susceptibility of the first magnetization curve give only a survey of the anhysteretic susceptibility variations.

Let reconsider now the analytical expression of E_m equation 22, temperature dependent parameters are: λ_{max}, χ_0 and M_s. K_1 quickly decreases while the temperature increases, meaning that the rotation becomes progressively dominant (for a temperature around 100°C up to 200°C). The maximum

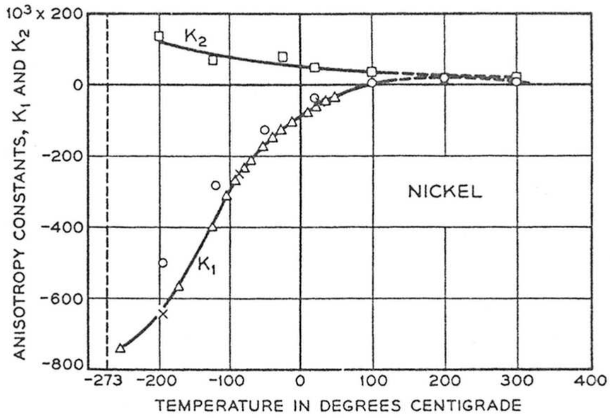

(a)

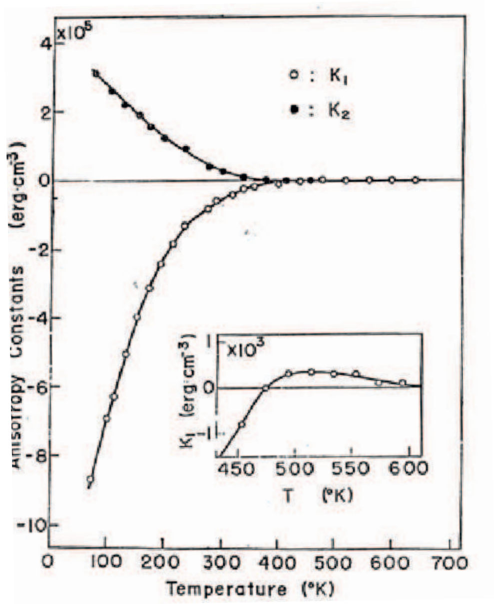

(b)

Figure 7: Effect of temperature on the magnetocrystalline constants of nickel - (a) results of Honda [6]; (b) results of Tatsumoto [24] - NB: K_1 and K_2 are given in erg/cm^3 - 10 [erg/cm^3] =1 [J/m^3].

magnetostriction definition has to be reconsidered because it tends progres-

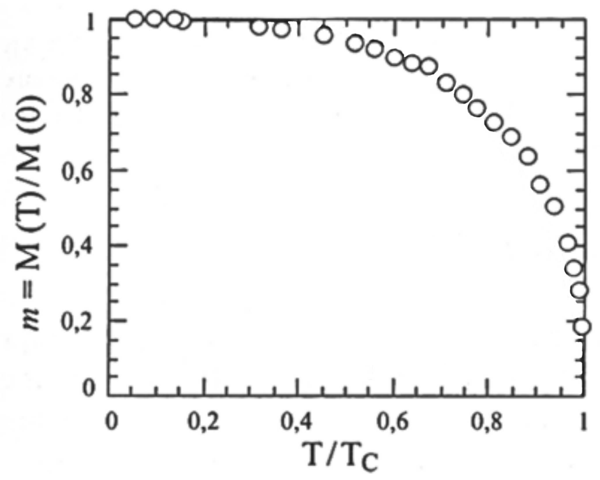

Figure 8: Effect of temperature on the saturation magnetization of nickel [25].

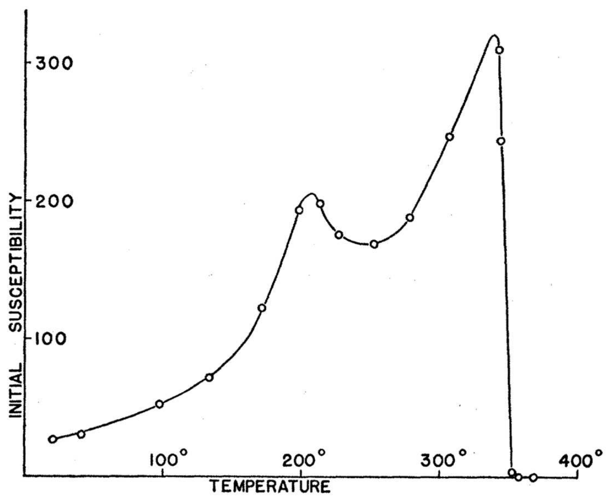

Figure 9: Effect of temperature on the initial susceptibility of nickel [22].

sively to the saturation magnetostriction:

$$\lambda_{max} = \frac{2}{5}\lambda_{100}k_a + \frac{3}{5}\lambda_{111}k_b \tag{36}$$

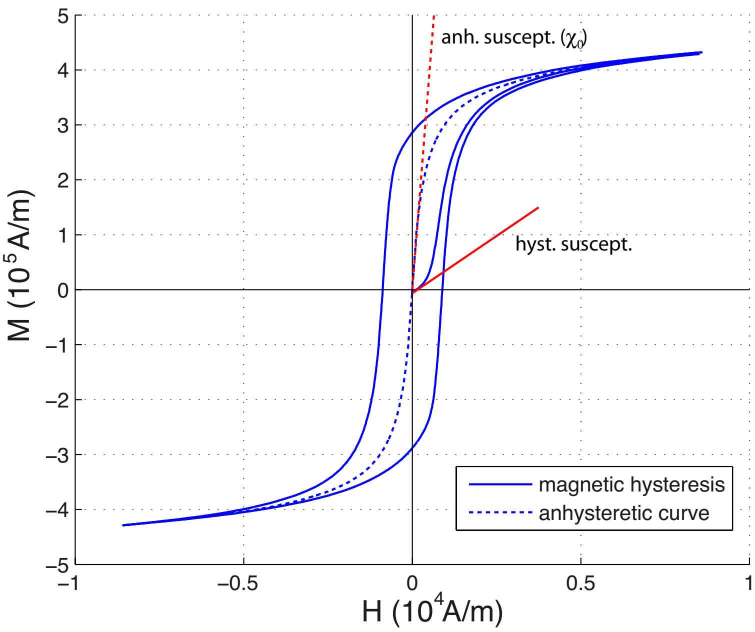

Figure 10: Typical cyclic and anhysteretic behaviors of pure polycrystalline nickel at RT.

Variations of λ_{100} and λ_{111} with temperature must be taken into account too. They are considered to follow the same variation with temperature than λ_s plotted in figure 6.

Variation of the anhysteretic initial susceptibility χ_0 with temperature is unknown since figure 9 refers to the hysteretic initial susceptibility. To simplify, a linear increasement of χ_0 with temperature is considered:

$$\chi_0(T) = \chi_0^{RT} \frac{T}{T^{RT}} \tag{37}$$

Such relation is in global accordance with the experimental variation of hysteretic initial susceptibility and allows a simplification of the magnetostriction modulus expression:

$$\frac{1}{E_m} = \frac{3\chi_0^{RT}}{5\mu_0} (\frac{\lambda_{max}(T)}{M_s(T)})^2 \tag{38}$$

Therefore new assessments of the magnetostriction modulus can be obtained considering the different previous estimations at a temperature of

200°C. Parameters values at this temperature come from experimental results. They are reported in table 4.

Table 4: Physical constants of pure nickel at 200°C used for the estimation of the apparent Young's modulus (a linear variation of the ideal Young's modulus with temperature has been used to estimate the C_{ij} values using equation (40) - Poisson's ratio variations are not considered); χ_0 is supposed unchanged with temperature.

M_s	λ_{100}	λ_{111}	χ_0	C_{11}	C_{12}	C_{44}
3.9×10^5	-33.3	-16.7	800	227	136	229
A/m	ppm	ppm	-	GPa	GPa	GPa

The effective Young's modulus E is 206 GPa at 200°C (in accordance with C_{ij} values and experimental results). Different estimations of the apparent Young's modulus can be made depending on the different estimations of k_a and k_b. They are reported in table 5.

Table 5: Different estimations of k_a, k_b, λ_{max}, E_m, E_a and $\Delta E/E(\%) = (E_a - E)/E \times 100$ at 200°C - magnetostriction is given in ppm ($\times10^{-6}$) and moduli in GPa - V: Voigt estimation, R: Reuss estimation, HS+: Hashin-Shtrikman upper estimation, HS-: Hashin-Shtrikman lower estimation, SC: self-consistent estimation.

	V	HS+	SC	HS-	R
k_a	0.525	0.687	0.719	0.773	1
k_b	1.316	1.209	1.187	1.151	1
λ_{max}	-20.2	-21.3	-21.5	-21.8	-23.3
E_m	977	881	863	835	731
E_a	170	167	166	165	161
$\Delta E/E(\%)$	-17.4	-19.0	-19.3	-19.8	-22.0

Whatever the estimation, a decreasement of the apparent Youngs modulus with temperature is clearly observed. This decreasement fluctuates between 36 MPa and 45 MPa depending on the estimation. These values are in good agreement with values observed in figure 3 and those reported in [6] (figure 4a and 4a after annealing). It can be noticed that the homogeneous stress estimation leads now to the lowest apparent Young's modulus (it was corresponding to the highest value for the calculations at RT). Homogeneous stress estimation allows to get the highest variation of ΔE effect with temperature. On the other hand it is interesting to compare these values with those reported in table 6, where the no rotation condition has been maintained. A clear increase of the apparent Young's modulus is observed, that does not fit to the experimental results. It confirms that the variation of the apparent Young's modulus with temperature is due to a combined effect of variation of intrinsic physical constants and a relaxation of the magnetization rotation enhancing the magnetostriction strain variation with stress.

The Young's modulus remains to its effective value (196 MPa) when temperature reaches the Curie temperature (disappearance of ferromagnetic coupling), leading to the sharp increase of apparent Young's modulus.

Table 6: Different estimations of k_b, λ_{max}, E_m, E_a and $\Delta E/E(\%) = (E_a - E)/E \times 100$ at 200°C **using the no-rotation condition:** $\lambda_{max} = \frac{3}{5}\lambda_{111}k_b$ - magnetostriction is given in ppm ($\times 10^{-6}$) and moduli in GPa - V: Voigt estimation, R: Reuss estimation, HS+: Hashin-Shtrikman upper estimation, HS-: Hashin-Shtrikman lower estimation, SC: self-consistent estimation.

	V	HS+	SC	HS-	R
k_b	1.316	1.209	1.187	1.151	1
λ_{max}	-13.2	-12.1	-11.9	-11.5	-10.0
E_m	2289	2715	2813	2993	3966
E_a	189	191	192	193	196
$\Delta E/E(\%)$	-8.3	-7.1	-6.8	-6.4	-4.9

4. Numerical implementation of $E(T)$ and comparisons between experiments and modeling

4.1. Multiscale model and simulation of apparent Young's modulus at the room temperature

The variations of nickel physical constants with temperature are now considered to propose a modeling of $E_a(T)$ curve and compare it to the measurements. The previous calculations used the assumption of no effect of magnetization rotation on the magnetostrictive response. This assumption is acceptable for a high K_1. When K_1 reaches 0, this assumption is not valid anymore. The analytical modeling can be made on the other hand when λ_{max} is known. The definition of λ_{max} is nevertheless not unique (known only for free rotation or no rotation situations). These different arguments motivate the choice of a numerical approach.

A multiscale (MS) model originally dedicated to build magneto-mechanical constitutive laws for anisotropic polycrystalline media is used [13]. The main characteristics of this model are recalled in Appendix A. MS model involves three scales: domain scale, grain scale and polycrystalline scale (representative volume element - RVE). Initially proposed by [26] at the grain scale, it was extended to polycrystals by [13] and [27]. In the present study, an isotropic grain distribution has been used (546 grains [13]). This model allows, among others, to simulate the ΔE effect of nickel ($\epsilon^{\mu}_{33}(\sigma)$) as reported in figure 11 where the effect of homogeneous stress or self consistent conditions are compared.

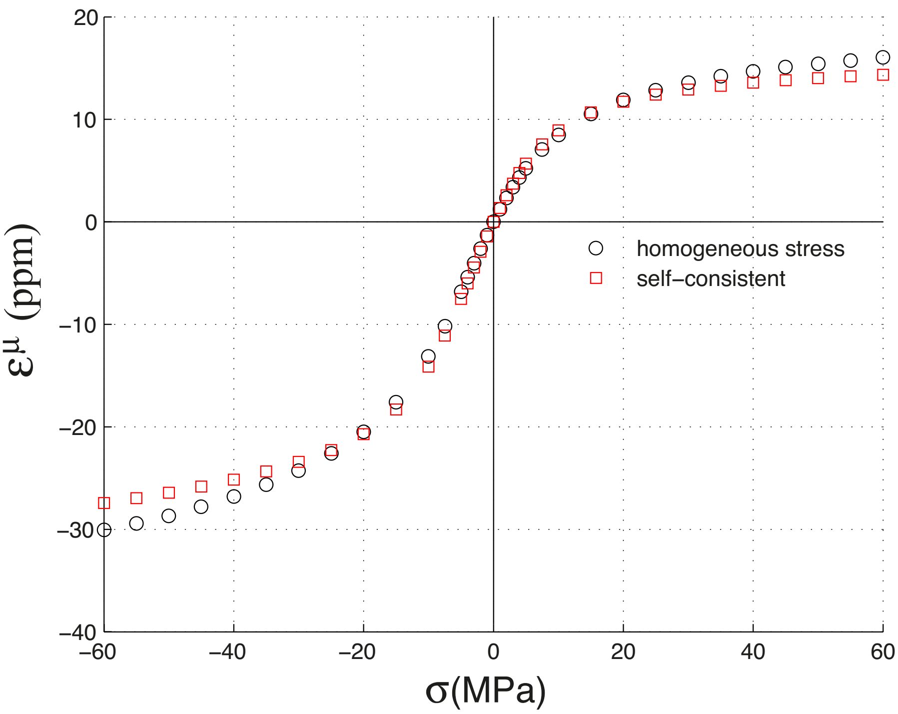

Figure 11: ΔE effect for isotropic polycrystalline nickel as estimated by MS model at RT for homogeneous stress and self-consistent conditions.

The difference of slope a zero applied stress between the two simulations is low: a slope of $1.212\times10^{-12}\mathrm{Pa}^{-1}$ is obtained for the homogeneous stress condition and of $1.345\times10^{-12}\mathrm{Pa}^{-1}$ for the self-consistent condition. These values correspond to E_m^{-1}. The corresponding apparent Young's modulus is evaluated to 176 GPa and 172 GPa respectively (for a ideal Young's modulus of 223 GPa). These values are lower than the experimental values at RT reported in figure 3 and different from the value obtained after the analytical approach (206 GPa for homogeneous stress estimation and 200 GPa for the self-consistent one) which considered that rotation was not occurring at RT. Another estimation by the analytical approach of the apparent Young's modulus at RT has been made, now considering a free rotation mechanism (*i.e.* $\lambda_{max} = \frac{2}{5}\lambda_{100}k_a + \frac{3}{5}\lambda_{111}k_b$). The different estimations of E_a (numerical and analytic approaches for homogeneous stress and self-consistent estimations) are reported in table 7. The analytical estimation considering a free magnetization rotation leads to results closer to the numerical solution than the no-rotation assumption, especially for the self-consistent estimation. The variation of magnetostriction with stress must be considered as the result of both wall displacement and magnetization rotation at RT.

Table 7: Various estimations of apparent Young's moduli E_a(GPa) T=20°C. R: homogeneous stress: SC: self-consistent

R num.	SC num.	R no rot.	SC no rot.	R rot.	SC rot.
176	172	206	200	154	162

4.2. Simulation of $E_a(T)$ for isotropic polycrystalline nickel

The simulation of the apparent Young's modulus with temperature requires to use relations between physical constants (ideal Young's modulus, magnetostriction, magnetocrystalline constant, saturation magnetization) and temperature. Some of these relations have a theoretical background, others have been built in former papers by different authors so that they fit properly the experimental data. The following functions are proposed:

- Ideal Young's modulus - All experiments (recent and former) show a linear decreasement of ideal Young's modulus E with temperature T.

The following linear relation is implemented in the model:

$$E = E_0 - k_0 T \tag{39}$$

with E_0=237.6 GPa: Young's modulus at 0K; k_0=0.06603 GPa/K. Figure 12 allows the comparison between the linear approximation and the experimental results. The same relation is used to consider the variation of C_{ij} stiffness constants with temperature (in the range of temperature considered in this paper):

$$C_{ij}(T) = C_{ij}(T^{RT})\frac{E(T)}{E(T^{RT})} \tag{40}$$

- Saturation magnetization - the theoretical variation of the saturation magnetization M_s with temperature is given by the self-consistent equation [32]:

$$\frac{M_s}{M_{s0}} = tanh(\frac{M_s/M_{s0}}{T/T_C}) \tag{41}$$

with M_{s0} the magnetization at 0K (M_{s0}=4.956×10^5 A/m). The temperature T is expressed in Kelvin.

Figure 13 allows the comparison between the experimental and modeled evolution of the saturation magnetization with the temperature. The model gives high quality results.

- Magnetocrystalline constants - The variation of magnetocrystalline constant K with temperature has been studied theoretically by Zener [28]. It is expressed as function of magnetization ratio, K^0 the magnetocrystalline constant at 0K, and a constant n:

$$K(T) = K^0(M_s/M_s^0)^n \tag{42}$$

n=10 for a cubic symmetry. This value is justified considering that the amplitude of magneto crystalline K_1 is higher than the amplitude of K_2, and considering the cubic symmetry (4^{th} order of direction cosines). This model is denoted model 1.

It has been shown that this relation did not fit very well the experimental results obtained for nickel. The relation has been modified by

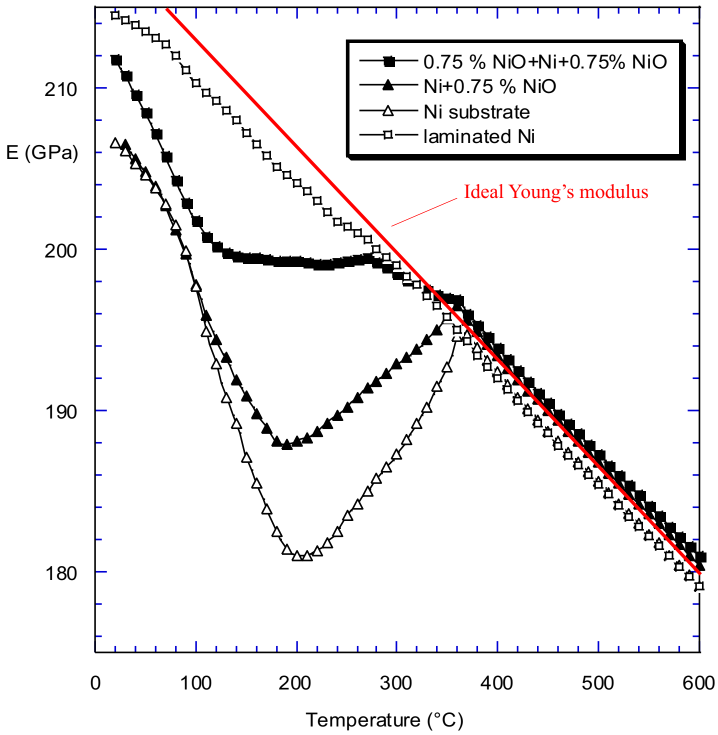

Figure 12: Variation of Young's modulus with temperature for different specimens complemented by a linear approximation of ideal Young's modulus.

533 Carr [30] to take account of the change of sign of K_1 and an earlier
534 decreasement of magneto crystalline amplitude. This model is denoted
535 model 2.

$$K(T) = K^0(\frac{M_s}{M_s^0})^n(1 - \alpha\frac{T}{T_C}) \tag{43}$$

536 with n=10 and $\alpha > 1$

Williams and Bozorth [6] proposed on the other hand to use the following empirical relation to define the evolution of magneto crystalline constants with temperature:

$$K(T) = K^0 exp(-kT^2) \tag{44}$$

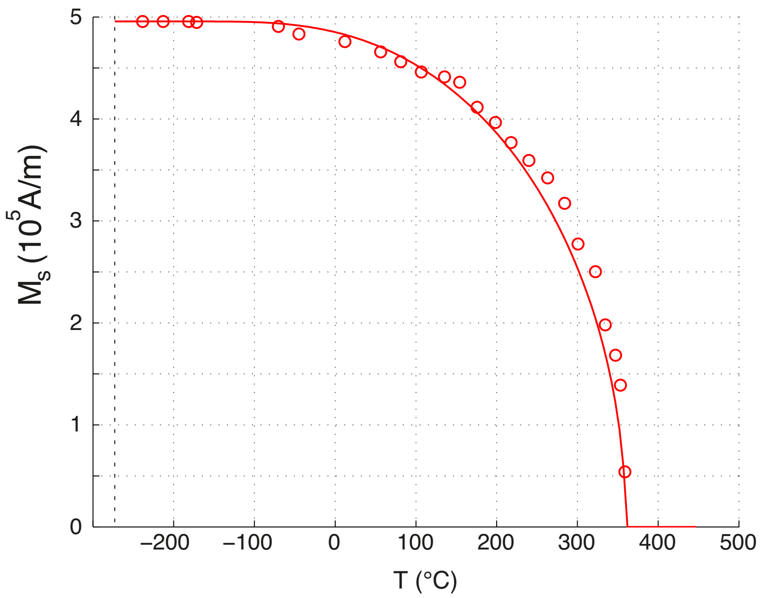

Figure 13: Comparison between experiment (circles) and modeling (full line - see eq. 41) of the evolution of saturation magnetization with temperature.

It has been decided to use this formulation multiplied by a linear function of temperature in order to represent the change of sign of K_1. This model denoted model 3 is given by:

$$K_1(T) = K_1^0 exp(-k_1 T^2)(1 - \alpha \frac{T}{T_C}) \tag{45}$$

with: K_1^0=-82$\times 10^3$ J/m^3, k_1=1.562$\times 10^{-5}$K^{-2}, $\alpha = 1.338$.
Figure 14 gathers experimental points from various authors [6, 24, 29] and the results of the three models. The figure 15 is a zoom of figure 14. Model 3 gives clearly the best results.

Following Williams and Bozorth [6], equation (46) has been used to model the variations of K_2 with temperature:

$$K_2(T) = K_2^0 exp(-k_2 T^2) \tag{46}$$

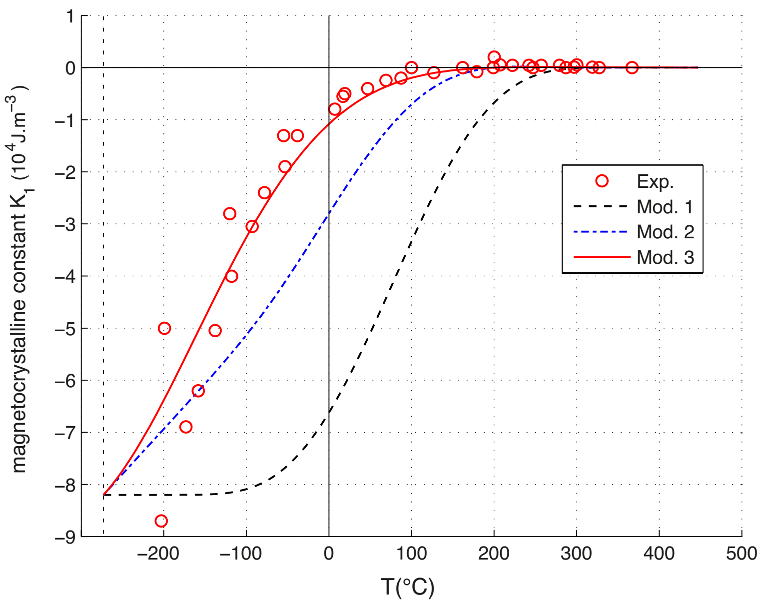

Figure 14: Comparison between experimental and modeled variation of K_1 with temperature.

with: K_2^0=±28 × 10^3 J/m^3, k_2=2.78×10^{-5}K^{-2}.

K_2^0 will be considered either positive or negative during the modeling since the sign of K_2 is controversial. Figure 16 gathers experimental points from various authors [6, 24] (including a negative estimation from [31]) and results of the model. The sensitivity of magnetostriction modulus to the K_2 sign has to be estimated to verify if this uncertainty is significant or not.

- Magnetostriction constants - No theoretical relation between magnetostriction and temperature is available in literature. A polynomial variation is chosen to model the saturation magnetization of isotropic polycristal:

$$\lambda_s(T) = \lambda_s^i(1 - (T/T_C)^m) \tag{47}$$

with λ_s^i=-32×10^{-6} and $m = 3.4$. Extension of this function to λ_{100} and λ_{111} constants is considered, leading to:

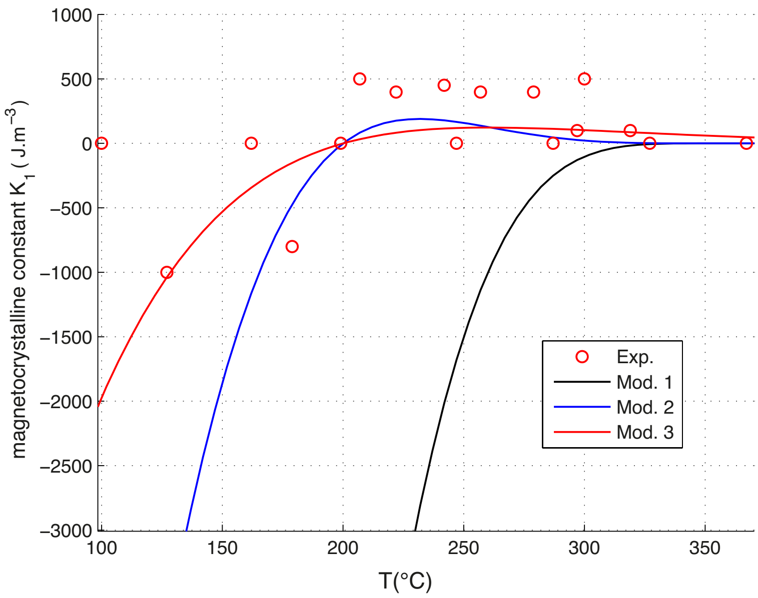

Figure 15: Comparison between experimental and modeled variation of K_1 with temperature - zoom of figure 14.

$$\lambda_{100}(T) = \lambda^i_{100}(1 - (T/T_C)^m) \tag{48}$$

$$\lambda_{111}(T) = \lambda^i_{111}(1 - (T/T_C)^m) \tag{49}$$

with λ^i_{100}=-54×10^{-6} and λ^i_{111}=-27×10^{-6} so that the values at RT correspond to classical values (-50×10^{-6} and -25×10^{-6} respectively). Results are plotted in figure 17 showing a good ability of the function to model the experimental data.

These various functions are introduced in the multiscale model (Appendix A). In order to estimate the magnetostriction modulus, the multiscale model is employed to model the effect of a small stress magnitude (*i.e.* $\Delta\sigma_{33}$=0.1MPa) on the magnitude of macroscopic magnetostriction $\Delta\epsilon^\mu_{33}$. It leads to:

$$\frac{1}{E_m} = \left.\frac{d\epsilon^\mu_{33}}{d\sigma}\right|_{\sigma=0} \approx \left.\frac{\Delta\epsilon^\mu_{33}}{\Delta\sigma_{33}}\right|_{\sigma_{33}=0} \tag{50}$$

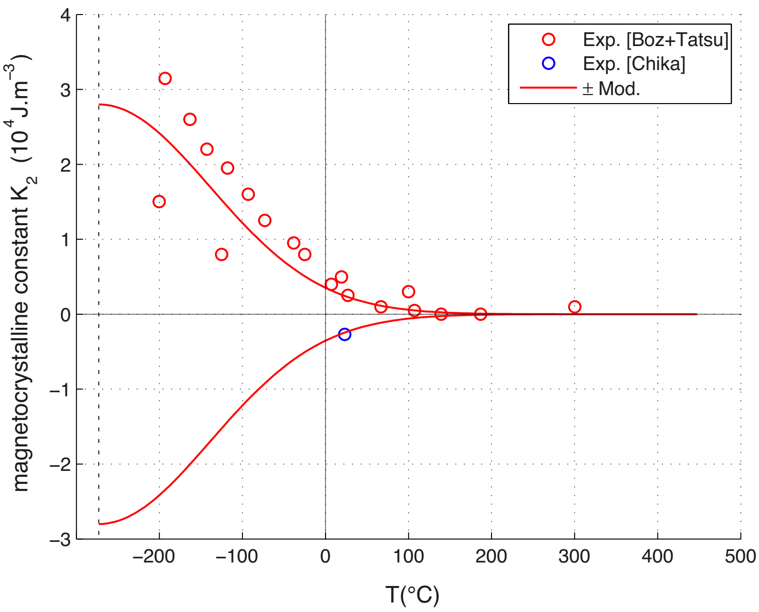

Figure 16: Comparison between experimental and modeled variation of K_2 with temperature.

The apparent Young's modulus E_a satisfies the rule of mixture:

$$\frac{1}{E_a} = \frac{1}{E} + \frac{1}{E_m} \tag{51}$$

The variation of apparent Young's modulus for isotropic polycrystalline nickel with temperature is finally plotted in figure 18 using a homogeneous stress assumption and in figure 19 for the self-consistent condition. Plotted curves correspond to multiscale model (MS), analytical model without rotation, and analytical model with free rotation. The results obtained using the MS model are qualitatively in good agreement with the experimental results with a first decreasement with temperature followed by a strong increasement up to the Curie temperature. The temperature corresponding to the minimum apparent Young's modulus is in accordance with experimental data. The global level of apparent Young's modulus is lower than expected from the room temperature up to 200°C, and the self-consistent approach leads to a clear underestimation of the Young's modulus variation. It can be observed by the way that the analytical model leads to a large (too large) frame

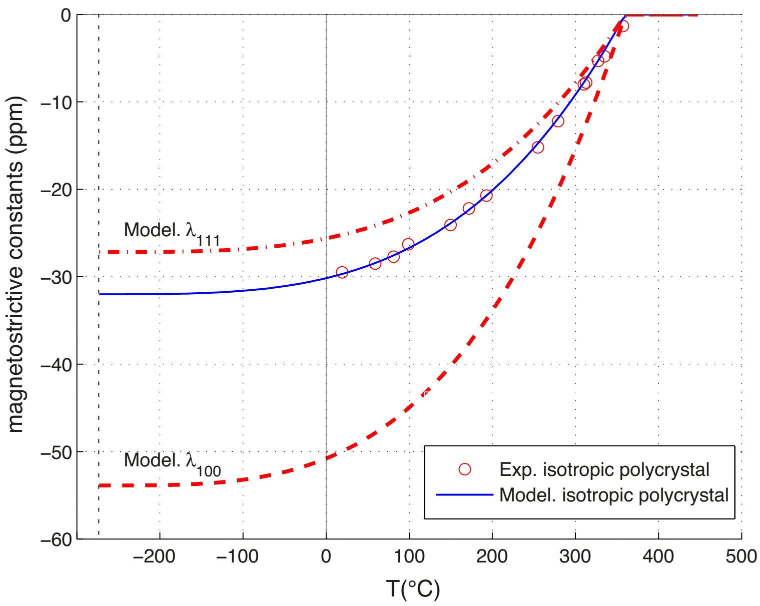

Figure 17: Comparison between experiment (circles) and modeling (full line) of the saturation magnetostriction with temperature. Representation of $\lambda_{100}(T)$ and $\lambda_{111}(T)$ functions.

of the MS solution in both cases for temperatures below 200°C. Above this temperature, analytical results do not frame the solution anymore (especially for the homogeneous stress estimation) indicating that the wall displacement mechanism hypothesis used to get the analytical modeling is not applicable any more. Since the homogeneous stress assumption gives results closer to experiments, it has been used for the next simulations.
Because of uncertainties concerning the K_2 anisotropy constant, it has been decided to simulate the situation where $K_2(T)$ is the exact opposite of previous function and the situation where $K_2(T) = 0$. Behaviors are plotted in figure 20 (using homogeneous stress condition). A very small change is observed meaning that K_2 is a second order parameter. It has been kept positive for the next simulations.

Reasons that explain the discrepancy between experiment and modeling are numerous: representativity of RVE, various uncertainties on physical values,.... The main drawback is associated to the high uncertainty on the variation of initial anhysteretic susceptibility with temperature and a possible anisotropic initial distribution of domains. It must finally be kept in mind

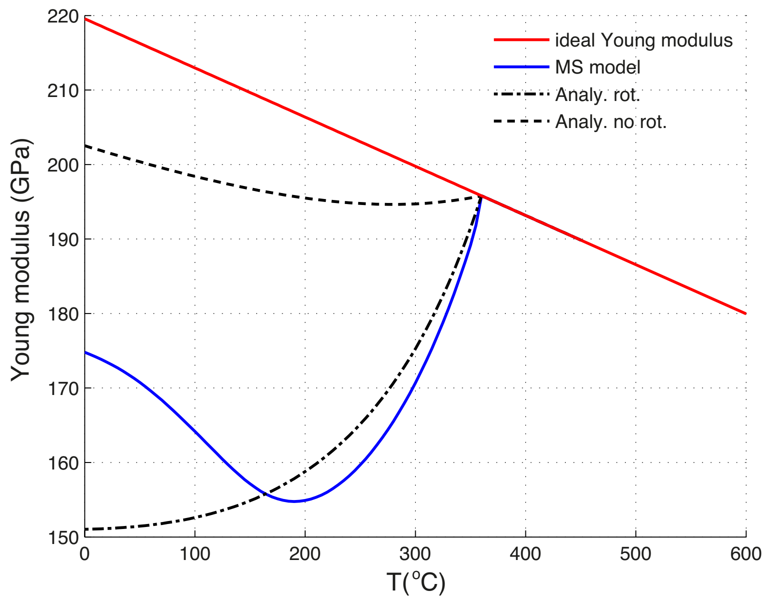

Figure 18: Change of nickel Young's modulus with temperature - ideal and apparent Young's modulus - homogeneous stress estimation.

that the mechanical loading used to measure the apparent Young's modulus cannot be considered as an *anhysteretic* loading, meaning that comparisons between modeling and experiments should be considered at this step as mainly qualitative comparisons, waiting for a hysteretic version of the modeling (see [33, 34] for propositions of extension to hysteretic modeling).

4.3. Simulation of NiO coating effects

The experimental measurements reported in figure 3 show that the "stiffening" effect magnitude below T_C highly varies depending on the sample state (as-received, two sides oxidized, single side oxidized, peeled-off oxide) to another. To highlight and explain that effect, the following points have to be considered:

- nickel has a larger dilatation coefficient than the oxide.
- oxide is formed at high temperature (T_{Ox}=1100°C).
- for any temperature below T_{Ox}, the oxide layer is in compression on the nickel.

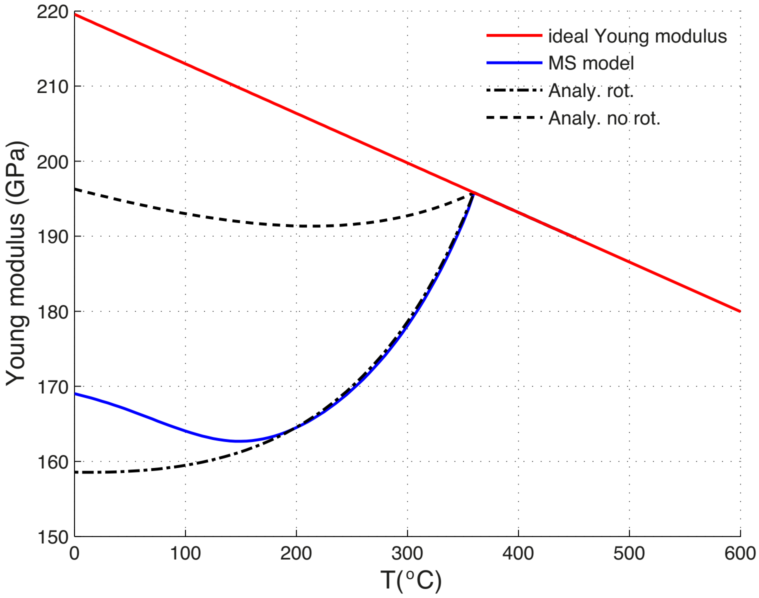

Figure 19: Change of nickel Young's modulus with temperature - ideal and apparent Young's modulus - self-consistent estimation.

- the mechanical balance states that the nickel layer is submitted to an equibitension residual stress of amplitude σ_0.

$$\boldsymbol{\sigma}_r = \begin{pmatrix} 0 & & \\ & \sigma_0 & \\ & & \sigma_0 \end{pmatrix}$$

Experimental XRD measurements reported in section 2.3 and provided at RT enable the estimation of σ_0 magnitude for the 1-side oxidized and the 2-sides oxidized situations. For NiO-Ni-NiO system, σ_0 is homogeneous in the nickel layer and has been estimated to +9 MPa. For Ni-NiO, stress is heterogeneous across the thickness. Overall the average value in the nickel layer has been estimated to +3 MPa. For a more accurate modeling, it must be taken into account that σ_0 depends on temperature since it decreases theoretically to zero at T_{Ox}. The following parametric formula can be used:

$$\sigma_0(T) = \sigma_0^0 - qT \tag{52}$$

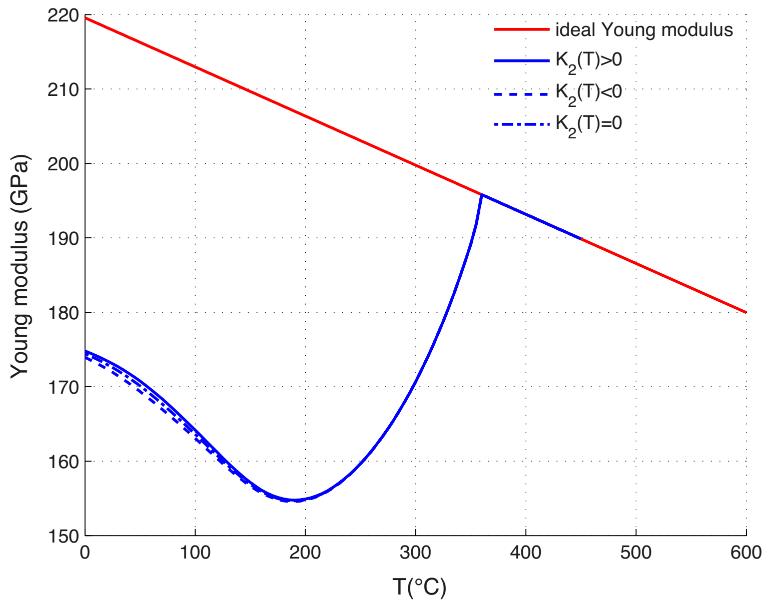

Figure 20: Change of nickel Young's modulus with temperature - effect of K_2 magneto crystalline constant - homogeneous stress estimation.

with σ_0^0=$\{11.42, 3.81\}$MPa and q=$\{8.25, 2.75\} \times 10^{-3}$MPa/K for the {2-sides oxidized , 1-side oxidized} situations respectively. $\sigma_0(T)$ functions are plotted in figure 21 in the temperature range of experiments.

The residual stress tensor is introduced in the multiscale model as a constant external loading (the relaxation of this stress with the magnetostriction strain of the sample is not considered). The procedure explained above is used to extract the magnetostriction modulus variations with temperature. Results are plotted in figure 22. The expected saturation effect is observed. The amplitude reduction is lower than observed experimentally. Uncertainties on the residual stress level and other approximations are probably at the origin of these discrepancies.

In order to estimate the sensitivity to higher stress, the model has been tested for a superimposed constant uniaxial applied stress $\sigma_{33} = \sigma_a$. Results are illustrated in figure 23 where σ_a varies from 5MPa to 50MPa exhibiting the mechanical saturation phenomenon already discussed in literature [6] and reported in figures 3 (as received material) and 4b (cold rolled sample).

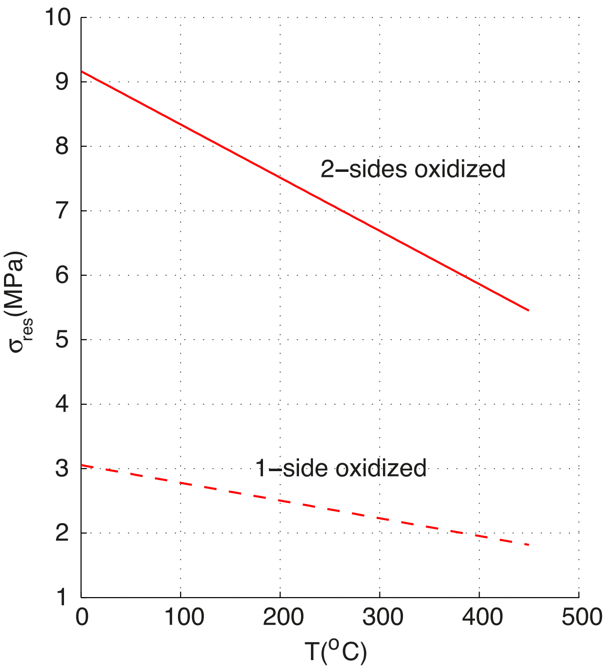

Figure 21: Evolution of residual stress associated to oxide layers with temperature.

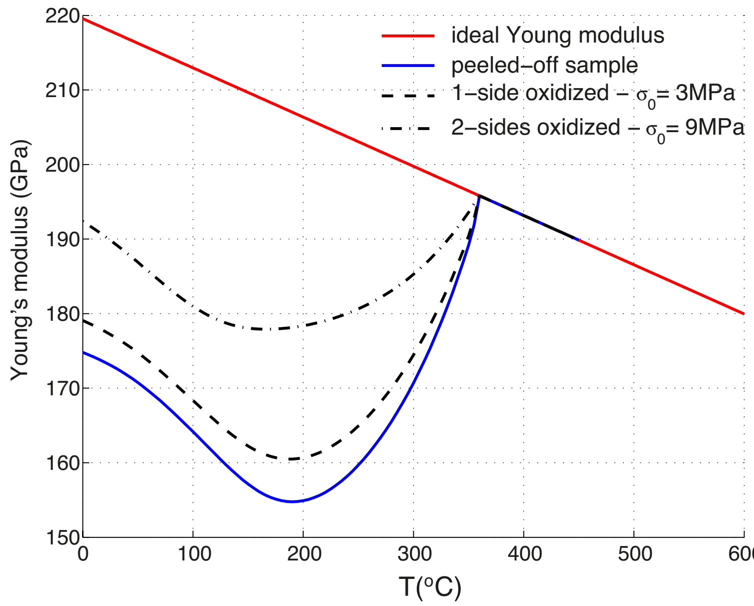

Figure 22: Influence of residual stress associated to oxide layers on the apparent nickel Young's modulus - homogeneous stress estimation.

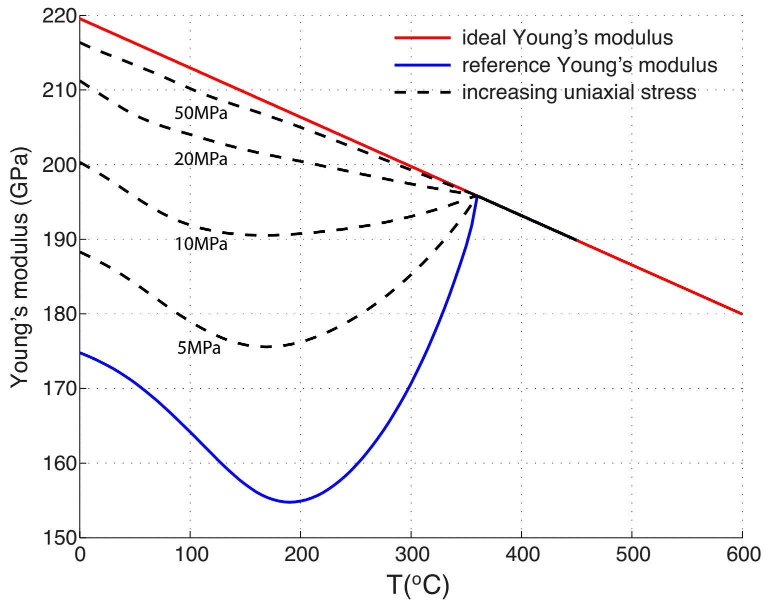

Figure 23: Change of nickel Young's modulus with temperature - effect of uniaxial applied stress - homogeneous stress estimation.

The model gives also the opportunity to test the influence of a magnetic field on the apparent Young's modulus of nickel. The effect of a superimposed constant magnetic field $H_3 = H_a$ is illustrated in figure 24. H_a varies from 1000A/m to 10000A/m exhibiting the magnetic saturation phenomenon already discussed in literature [6] and reported in figure 4a.

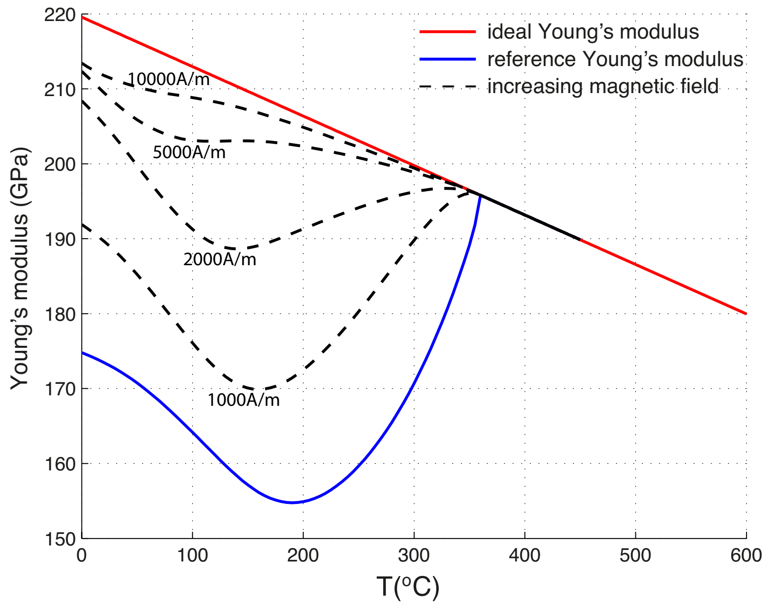

Figure 24: Change of nickel Young's modulus with temperature - effect of constant applied magnetic field - homogeneous stress estimation.

5. Conclusion

In this work a modeling of the variation of Young's modulus with temperature of Ni and Ni-NiO layers has been proposed. The magnetic origin of this behavior has first been underlined, justifying the use of a magneto mechanical approach for the modeling. A first analytical modeling includes the change of the saturation magnetization, of the initial anhysteretic susceptibility and of the maximal magnetostriction with a relaxation of magneto-crystalline anisotropy concomitant to increasing temperature. The second modeling is a numerical modeling giving the average behavior of a representative volume element composed of 546 regularly distributed grains. This modeling requires

to define the temperature dependence of many magnetic and magnetostrictive parameters. It allows a continuous description of the change of Young's modulus with temperature.
The discrepancies observed with experiments concern the lower level of Young's modulus at room temperature up to 200°C (as observed for peeled-off, 1-side oxidized or 2-sides oxidized sample). Discrepancies can be explained mainly by the fact that the modeling is reversible although the physical phenomenon is irreversible (hysteresis effect) and that the variation of initial anhysteretic susceptibility with temperature remains unknown. Other uncertainties and approximations (infinite medium) are additive reasons.
It has also been shown that even if crystallographic texture remains roughly isotropic after oxidizing at 1100°C, the grain size increases drastically for high duration heat treatments [4]. This size may reach the thickness of the layer leading to a surface effect whose magnetic and magnetostrictive consequences have been extensively discussed in [36]. This surface effect may have important consequences on the global response of apparent elastic behavior because the domain structure is strongly modified by free surface conditions. The analysis proposed in this paper remains nevertheless sufficient to understand now clearly how the Ni-NiO system behaves. An extension to another *Ni / coating* system or more generally another *ferromagnetic substrate / coating* system is possible, opening to a wide range of applications. It could be for example applied to the measurement of thickness deposits and/or to the inverse identification of internal stress levels inside a substrate.

6. acknowledgements

The authors wish to thank Jocelyne Balmain, LaSIE UMR 7356 CNRS, Université de La Rochelle, for her careful preparation of oxidized samples.

Appendix A. Multiscale modeling

The multiscale model involves three scales: domain scale, grain scale and polycrystalline scale (representative volume element - RVE). It is especially dedicated to estimate the macroscopic magnetization and magnetostrictive responses to macroscopic magnetic field and/or stress loadings of polycrystalline anisotropic media. Initially proposed by [26] at the grain scale, it was extended to polycrystals by [13] and [27]. In the present study, it is used to model the variation of magnetostriction with respect to stress ($d\epsilon^{\mu}/d\sigma$ - ΔE effect) considering:

- free specimen (peeled-off sample)
- 1-side oxidized sample (biaxial stress - σ_0=3MPa)
- 2-sides oxidized sample (biaxial stress - σ_0=9MPa)
- increasing uniaxial stress on a sample
- increasing magnetic field on a sample

An isotropic grain distribution has been used. Since this model always refers to equilibrium, modeling results must be compared to anhysteretic (reversible) experimental measurements.

Appendix A.1. Micromagnetic model (grain scale)

A polycrystalline ferromagnetic media can be considered as an aggregate of single crystals assemblied following the orientation data. The microscopic model proposed by [26] is written using the volumetric fraction f_α of each domain family α (six $< 100 >$ or height $< 111 >$ families depending on easy directions), and magnetization rotation (two angles θ_α and ϕ_α per domain family) as internal variables. The potential energy (A.1) is defined for each magnetic domain family α as the sum of the magneto-crystalline (A.2), magnetostatic (A.3) and elastic (A.4) energies, detailed hereafter.

$$W^{\alpha} = W^{\alpha}_{K} + W^{\alpha}_{H} + W^{\alpha}_{\sigma} \tag{A.1}$$

$$W^{\alpha}_{K} = K_1(\gamma_1^2\gamma_2^2 + \gamma_2^2\gamma_3^2 + \gamma_3^2\gamma_1^2) + K_2(\gamma_1^2\gamma_2^2\gamma_3^2) \tag{A.2}$$

$$W_H^\alpha = -\mu_0 \vec{H}^\alpha . \vec{M}^\alpha \tag{A.3}$$

$$W_\sigma^\alpha = \frac{1}{2}\boldsymbol{\sigma}^\alpha : \mathbb{C}^{\alpha-1} : \boldsymbol{\sigma}^\alpha \tag{A.4}$$

where $\vec{M}^\alpha = M_s \vec{\gamma}^\alpha$ is the magnetization vector of the domain family α (M_s: saturation magnetization), $\vec{\gamma}^\alpha$ denotes the direction of magnetization (γ_i^α: direction cosines) in the crystal frame. K_1 and K_2 are the magnetocrystalline energy constants. $\vec{H}^\alpha$ is the magnetic field at the domain scale. $\boldsymbol{\sigma}^\alpha$ is the stress tensor at the domain scale. $\mathbb{C}^\alpha$ denotes the stiffness tensor of a domain family (or grain $\mathbb{C}^g = \mathbb{C}^\alpha$). Homogeneous field and deformation assumptions lead to a definition of magneto static and elastic energies involving magnetic and mechanical loadings at the grain scale:

$$W_H^\alpha = -\mu_0 \vec{H}^g . \vec{M}^\alpha \tag{A.5}$$

$$W_\sigma^\alpha = -\boldsymbol{\sigma}^g : \boldsymbol{\epsilon}_\mu^\alpha \tag{A.6}$$

where $\boldsymbol{\epsilon}_\mu^\alpha$ denotes the magnetostriction strain tensor of a domain family α, where λ_{100} and λ_{111} are the magneto-elastic constants:

$$\boldsymbol{\epsilon}_\mu^\alpha = \frac{3}{2}\begin{pmatrix} \lambda_{100}(\gamma_1^2 - \frac{1}{3}) & \lambda_{111}\gamma_1\gamma_2 & \lambda_{111}\gamma_1\gamma_3 \\ \lambda_{111}\gamma_1\gamma_2 & \lambda_{100}(\gamma_2^2 - \frac{1}{3}) & \lambda_{111}\gamma_2\gamma_3 \\ \lambda_{111}\gamma_1\gamma_3 & \lambda_{111}\gamma_2\gamma_3 & \lambda_{100}(\gamma_3^2 - \frac{1}{3}) \end{pmatrix}_{CF} \tag{A.7}$$

At the grain scale, the volume fraction f_α of a family domain α is calculated using a statistical approach (Boltzmann function - A.8) [37] assuming that a magnetic domain is much smaller than a representative volume element (considered as a small body immersed into a large closed thermodynamic system). θ_α and ϕ_α are the results of a minimization of the potential energy of a domain family (A.10).

$$f_\alpha = \frac{\exp\left(-A_s . W^\alpha\right)}{\sum\limits_\alpha \exp\left(-A_s . W^\alpha\right)} \tag{A.8}$$

with

$$A_s = \frac{3\chi_0}{\mu_0 M_s^2} \tag{A.9}$$

$$\{\theta_\alpha, \phi_\alpha\} = min(W^\alpha) \tag{A.10}$$

χ_0, M_s and μ_0 are the initial anhysteretic susceptibility (model expressed in reversible condition), the saturation magnetization and the vacuum permeability respectively. This formulation uses the assumption that initial magnetization process is due to magnetic wall displacement and that rotation mechanism is neglected. This assumption is true for nickel at RT. An increasing temperature may compromise this hypothesis (especially when K_1 is reduced, that enhances the rotation mechanism).

A_s, through its relation with χ_0, is a parameter that accounts for energetic terms not considered in the final expression (exchange energy, magneto static phenomena). Its expression evolves with temperature since saturation magnetization and initial anhysteretic susceptibility are temperature dependent. Moreover, a global inverse proportionality dependence to temperature should be considered for A_s following the reference statistical approach [37], leading to the final expression:

$$A_s = \frac{3\chi_0(T)}{\mu_0 M_s(T)^2} \frac{T^{RT}}{T} \tag{A.11}$$

with T^{RT} the room temperature.

Assuming that the elastic behavior is homogeneous within a grain, the magnetostriction strain of a single crystal is written as the mean magnetostriction over the domains (A.12). The magnetization in a grain is defined as well (A.13).

$$\boldsymbol{\epsilon}_\mu^g =< \boldsymbol{\epsilon}_\mu^\alpha >= \sum_\alpha f_\alpha \, \boldsymbol{\epsilon}_\mu^\alpha \tag{A.12}$$

$$\vec{M}^g =< \vec{M}^\alpha >= \sum_\alpha f_\alpha \, \vec{M}^\alpha \tag{A.13}$$

The discrete approach has been modernized by [27]. In this new version, the easy directions are not defined *a priori*. The possible directions $\vec{\gamma}^\alpha$ are described through the mesh of a unit radius sphere (N unit vectors $\vec{x}_n$). A

34635 points mesh has been used in the present study. This new approach avoids the minimization operation A.10 and is less time consuming.

Appendix A.2. Localization and homogenization

Previous calculations are made for each grain of the polycrystalline aggregate. The polycrystalline aggregate considered in the study is a regularly distributed orientation data file made of 546 orientations [13]. The magnetic behavior at the polycrystalline scale is defined as the average value of magnetization (A.14). A local demagnetizing field in each grain due to the magnetization of the surrounding grains can be introduced [13, 36]: the magnetic field at the grain scale $\vec{H}^g$ is defined as a function of the external field, the mean secant equivalent susceptibility of the material χ_m, ($\chi_m = M/H$) and the difference between the mean magnetization $\vec{M}$ and the magnetization at the grain scale $\vec{M}^g$ (A.15). The elastic behavior is obtained using a self-consistent homogenization scheme. The macroscopic magnetostriction strain (A.16) is estimated using the Eshelby's solution and considering the local magnetostriction as a free strain; $\mathbb{B}^g$ denotes the fourth order stress concentration tensor.

$$\vec{M} =< \vec{M}^g > \tag{A.14}$$

$$\vec{H}^g = \vec{H} + \frac{1}{3 + 2\chi_m}(\vec{M} - \vec{M}^g) \tag{A.15}$$

$$\boldsymbol{\epsilon}_\mu =<^t \mathbb{B}^g : \boldsymbol{\epsilon}_\mu^g > \tag{A.16}$$

The magnetostriction strain at the grain scale is elastically incompatible and creates a stress that changes the magneto-elastic energy term (self-stress). The stress at the grain scale $\boldsymbol{\sigma}^g$ is derived from the implicit equation (A.17).

$$\boldsymbol{\sigma}^g = \mathbb{B}^g : \boldsymbol{\sigma} + \mathbb{C}^{acc} : (\boldsymbol{\epsilon}_\mu - \boldsymbol{\epsilon}_\mu^g) \tag{A.17}$$

with the accommodation stiffness tensor:

$$\mathbb{C}^{acc} = ((\mathbb{C}^g)^{-1} + (\mathbb{C}^\star)^{-1})^{-1} \tag{A.18}$$

and the stress concentration tensor:

$$\mathbb{B}^g = \mathbb{C}^g : (\mathbb{C}^g + \mathbb{C}^\star)^{-1} : (\mathbb{C}^0 + \mathbb{C}^\star) : (\mathbb{C}^0)^{-1} \tag{A.19}$$

$\mathbb{C}^\star = \mathbb{C}^0 : ((\mathbb{S}^{Esh})^{-1} - \mathbb{I})$ is the Hill's constraint tensor. $\mathbb{C}^0$ is the stiffness tensor of the effective medium. If a self-consistent scheme is chosen, $\mathbb{C}^0$ refers to the self-consistent stiffness tensor. $\boldsymbol{\sigma}$ is the macroscopic stress. $\mathbb{S}^{Esh}$ is the so-called Eshelby tensor, calculated following Mura [35].

References

[1] N.P. Padture, M. Gell, E.H. Jordan, *Science* **296** (2002), pp. 280-284.

[2] X.Q. Cao, R. Vassen, D. Stoever, *J. Eur. Ceram. Soc.* **24** (2004) pp.1-10.

[3] S.Guo, Y.Kagawa, *Scripta Materialia* **50** (2004), pp.1401-1406.

[4] M.Tatat, PhD Thesis, ENSMA, 2012.

[5] M. Tatat, P. Gadaud, P.-O. Renault, J. Balmain, C. Coupeau, X. Milhet, *Mat. Sci. Eng. A*, **571** (2013) pp.92-94.

[6] Bozorth R.M., "Ferromagnetism", *ed. D. Van Norstand*, N.Y. 1951.

[7] Cullity B.D., "Introduction to magnetic materials", *ed. Addison-Wesley*, N.Y. 1972.

[8] H. M. Ledbetter, R. P. Reed, *J. Phys. Chem. Ref. Data*, **2**, 3, (1973), pp.531-617.

[9] S. Siegel, L. Quimby, *Phys. Rev.*, **49**, (1936) pp.663-670.

[10] A.M. Huntz, *Mater. Sci. Eng. A* **201** (1995) pp.211-228.

[11] O. Hubert, L.Daniel, *J. of Magn. and Magn. Mater.*, **323** (2011), pp.1766-1781.

[12] L. Daniel, O. Hubert, *Eur. Phys. J. - Appl. Phys.*, **45** (2009) 31101.

[13] L. Daniel, O. Hubert, N. Buiron, R. Billardon. *J.of the Mech. and Phys. of Solids*, **56** (2008), pp.1018-1042

[14] P. Gadaud, *Int. J. Mater. Prod. Technol.* **26** (2006), pp.238-326.

[15] ASTM E 1876-00, *Annual Book of ASTM Standards*, 03.01 (2001), pp.1099-1112.

[16] V. Hauk, "Structural and Residual Stress Analysis by Non-destructive Methods: Evaluation, Application, Assessment", *ed. Elsevier*, Amsterdam,The Netherlands, (1997).

[17] G. Simons and H. Wang, "Single Crystal Elastic Constants and Calculated Aggregate Properties: A HANDBOOK", second Edition, *The M.I.T. Press*, Cambridge, Massachusetts, and London, England, (1971).

[18] A. Aubry, F. Armanet, G. Beranger, J.L. Lebrun, G. Maeder, *Acta Metall.*, **36** (1988) pp.2779-2786.

[19] C. Liu, A.M. Huntz, J.L. Lebrun, *Mater. Sci. Eng. A* **160** (1993), pp.113-126.

[20] O. Hubert, R. Waberi, S. Lazreg, K. Huyn-Soo, R. Billardon, "Measurement and two-scales modeling of the ΔE effect", in: 7th EUROMECH Solid Mechanics Conference, 2009.

[21] M. Bornert, T. Bretheau, P. Gilormini, "Homogenization in Mechanics of Material", *ed. Iste Publishing Company*, 2007.

[22] D. Kirkham, *Phys. Rev.* **52**, (1937), pp.1162-1167.

[23] E.Tatsumoto, T.Okamoto, Y.Kadena - *J. of the Physical Society of Japan*, **20** - Issue 8, (1965), pp. 1534-1534.

[24] E. Tatsumoto, T. Okamoto, N. Iwata, Y. Kadena, *J. of the Physical Society of Japan*, **20** - Issue 8, (1965), pp. 1541-1542.

[25] E. Ascher, *Helvetica Physica Acta*, **39** (1966), pp. 466-476.

[26] N. Buiron, L. Hirsinger, R. Billardon, *J. Phys. IV* **11** (2001) pp.373.

[27] N. Galopin, L.Daniel, *Eur. Phys. J. - Appl. Phys.*, **42** (2008) pp.153-159.

[28] C. Zener, *physical review*, **96**, num. 5, (1935), pp. 1335-1338.

[29] J. J. M. Franse, *Journal de Physique - C1* **32**, supplément au no 2-3, (1971), pp.186-192

[30] W.J. Carr, *J. appl. phys.*, **29** (1958), pp.436-437.

[31] S. Chikazumi, "Physics of Ferromagnetism", second ed., *Oxford University Press*, 1997.

[32] E. Du Trémolet de Lacheisserie, D.Gignoux, M.Schlenker, " Magnetism-I", *Springer Science & Business Media*, 2005.

[33] H. Hauser, *J. Appl. Phys.*, **96** (5) (2004), pp. 2753-2767.

[34] L. Daniel, M. Rekik, O. Hubert, *Arch. of Appl. Mech.*: Volume 84, Issue 9 (2014), pp.1307-1323.

[35] T. Mura, "Micromechanics of Defects in Solids", ed. *Martinus Nijhoff Publishers*, Dordrecht, MA, 1982.

[36] O. Hubert, L.Daniel, *J. of Magn. and Magn. Mater.*, **320** (2008), pp.1412-1422.

[37] A. Sommerfeld, "Thermodynamics and Statistical Physics", *Academic Press*, N.Y., 1955.